BioMedInformatics

MDPI

Article

The EGR1-FOS Transcriptional Axis in Liver Fibrosis: An Integrated Bioinformatic Analysis of Disease Progression and Shared Molecular Signatures in Cirrhosis

Youssef Nadir [1,*], Hicham Esselmani [1], Anass Oukhdouch [2,3], Habiba Nechchadi [4], Rahma Ennadi [1], Mohammed Amine Lkousse [5], Issame Farouk [6], Mustapha Najimi [7,8,†] and Mohamed Merzouki [1,†]

1 Biological Engineering Laboratory, Faculty of Science and Technology, Sultan Moulay Slimane University, Beni Mellal 23000, Morocco; esselmani1@yahoo.fr (H.E.); rahma.ennadi@gmail.com (R.E.); m.merzouki@usms.ma (M.M.)
2 Morphoscience Research Laboratory, Faculty of Medicine and Pharmacy, Cadi Ayyad University, Marrakesh 40000, Morocco; a.oukhdouch.ced@uca.ac.ma
3 Anatomic Pathology Department, University Hospital Mohammed VI, Marrakesh 40000, Morocco
4 Department of Biology, Polydisciplinary Faculty, Sultan Moulay Slimane University, Beni Mellal 23000, Morocco; habiba.nechchadi@gmail.com
5 Faculty of Medicine and Pharmacy of Beni Mellal, Sultan Moulay Slimane University, Beni Mellal 23000, Morocco; medamine.lko@gmail.com
6 Faculty of Medicine and Pharmacy Laayoune, Ibn Zohr University, Laayoune 70000, Morocco; issame.farouk@gmail.com
7 Laboratory of Pediatric Hepatology and Cell Therapy, Institute of Experimental and Clinical Research, 1200 Brussels, Belgium; mustapha.najimi@uclouvain.be
8 Private University of Marrakesh, Marrakesh 42312, Morocco
* Correspondence: youssef.nadir.phd@gmail.com
† These authors contributed equally to this work.

Abstract

Background: Liver fibrosis arises from chronic liver injury and remains a major clinical challenge due to its progression toward cirrhosis and hepatocellular carcinoma, as well as the absence of approved antifibrotic therapies. This study aimed to characterize the transcriptomic behavior of the EGR1-FOS axis in liver fibrosis and its evolution into hepatocellular carcinoma, and to identify genes shared between liver fibrosis and cirrhosis. **Methods**: An integrated bioinformatics approach was applied to GEO transcriptomic datasets. Differentially expressed genes in hepatic fibrosis were identified using GSE139602, GSE84044, and GSE49541, with GSE62232 as control when needed, while GSE14323 and GSE89377 were used to detect genes common with cirrhosis. GEPIA, TIMER, and TISCH2 were used to assess the involvement of the EGR1-FOS axis in hepatocellular carcinoma. External validation of EGR1 expression dynamics and its coregulation with FOS was performed using the GSE135251 dataset. **Results**: Eleven hub genes were identified, with emphasis on the EGR1-FOS axis. EGR1 expression fluctuated across liver fibrosis etiologies, whereas FOS was predominantly downregulated. A strong correlation between EGR1 and FOS (r = 0.77) was observed, remaining stable across fibrosis stages (all $p < 0.001$) and in hepatocellular carcinoma (r = 0.698, $p = 1.81 \times 10^{-55}$). Despite overall downregulation, both genes increased progressively with advancing fibrosis (EGR1: $p = 0.0008$–0.0035; FOS: $p = 0.0001$–0.0188). Four genes were shared between fibrosis and cirrhosis (SOX9, CD24, CXCR4, and CYP2C19). **Conclusions**: The EGR1-FOS axis acts as a dynamic regulator of liver fibrosis and its progression, and both this axis and the four shared genes identified may serve as valuable biomarkers and potential therapeutic targets.

Check for updates

Academic Editor: Burghardt Wittig

Received: 12 December 2025
Revised: 12 April 2026
Accepted: 13 April 2026
Published: 22 April 2026

Copyright: © 2026 by the authors. Licensee MDPI, Basel, Switzerland. This article is an open access article distributed under the terms and conditions of the Creative Commons Attribution (CC BY) license.

Keywords: liver fibrosis; liver cirrhosis; bioinformatic analysis; transcription factors; HCC; molecular signaling pathways; EGR1; FOS

1. Introduction

Liver fibrosis (LF) is a response to chronic damage originating from various sources. It is marked by the abnormal deposition of the extracellular matrix (ECM) driven by hepatic stellate cell (HSC) activation, which is the key component of its development and progression [1,2]. The activation of HSCs in response to pro-inflammatory molecules released by different cell types plays a central part in the pathogenesis of LF. Understanding the mechanisms of this activation and the genes that participate in it is essential for the development of innovative therapies [3]. Globally, it represents a major public health issue because of the life-threatening nature of the disease, as it progresses to advanced stages such as liver cirrhosis (LC), which itself evolves into hepatocellular carcinoma (HCC) [4]. LC is a complication of advanced hepatic fibrosis with a global mortality rate of 2.4%. It is categorized as compensated cirrhosis, due to the absence of symptoms and complications, and decompensated cirrhosis, which represents the symptomatic phase [5]. Despite progress in understanding the mechanisms implicated in LF and cirrhosis, as well as their progression to HCC, the management of these conditions is still limited to the management of symptoms and complications, and further investigations are required to explore the molecular framework in order to identify new biomarkers and innovative therapies [6].

The identification of gene candidates and pathways in LF in previous bioinformatic analyses was influenced by the use of single datasets and, in some studies, by the integration of human and animal data, which may reduce the direct translational relevance for human biomarker discovery. Although murine models are essential for mechanistic studies, important interspecies differences exist in hepatic gene expression and regulatory programs, and no single murine model fully reproduces the etiologic and molecular complexity of human LF. Therefore, to reduce cross-species bias and improve clinical relevance, we focused exclusively on human transcriptomic datasets in the discovery phase of this study [7,8]. The complexity of LF and its progression to hepatic cirrhosis requires further bioinformatics-driven and experimental studies to identify novel molecular biomarkers that could improve management and therapeutic interventions. The use of bioinformatic analyses allows researchers to analyze public datasets from repositories such as Gene Expression Omnibus (GEO). Integrating microarray and mRNA sequencing data from multiple studies helps gain a deeper understanding of liver diseases and overcome their limitations.

In our bioinformatic analysis, we used three public datasets (GSE139602, GSE84044, and GSE49541) for LF to identify the differentially expressed genes (DEGs) in LF compared to normal liver samples. Because two LF datasets lacked internal controls, platform-matched controls from the GEO dataset GSE62232 were used. The protein–protein interaction network was employed to screen for hub genes. The Gene Expression Profiling Interactive Analysis (GEPIA) platform was used to assess EGR1-FOS axis expression and its association with overall survival in HCC. To better understand its biological relevance, we explored immune infiltration and single-cell expression patterns of EGR1 and FOS using the Tumor IMmune Estimation Resource (TIMER) and TISCH databases. To validate the fluctuations in EGR1 and FOS expression and evaluate their coregulatory potential during different stages of LF, an external validation was performed using the GEO dataset GSE135251. Two datasets (GSE14323 and GSE89377) for LC were used to identify genes common to both LF and LC as the second objective of our study (Figure 1).

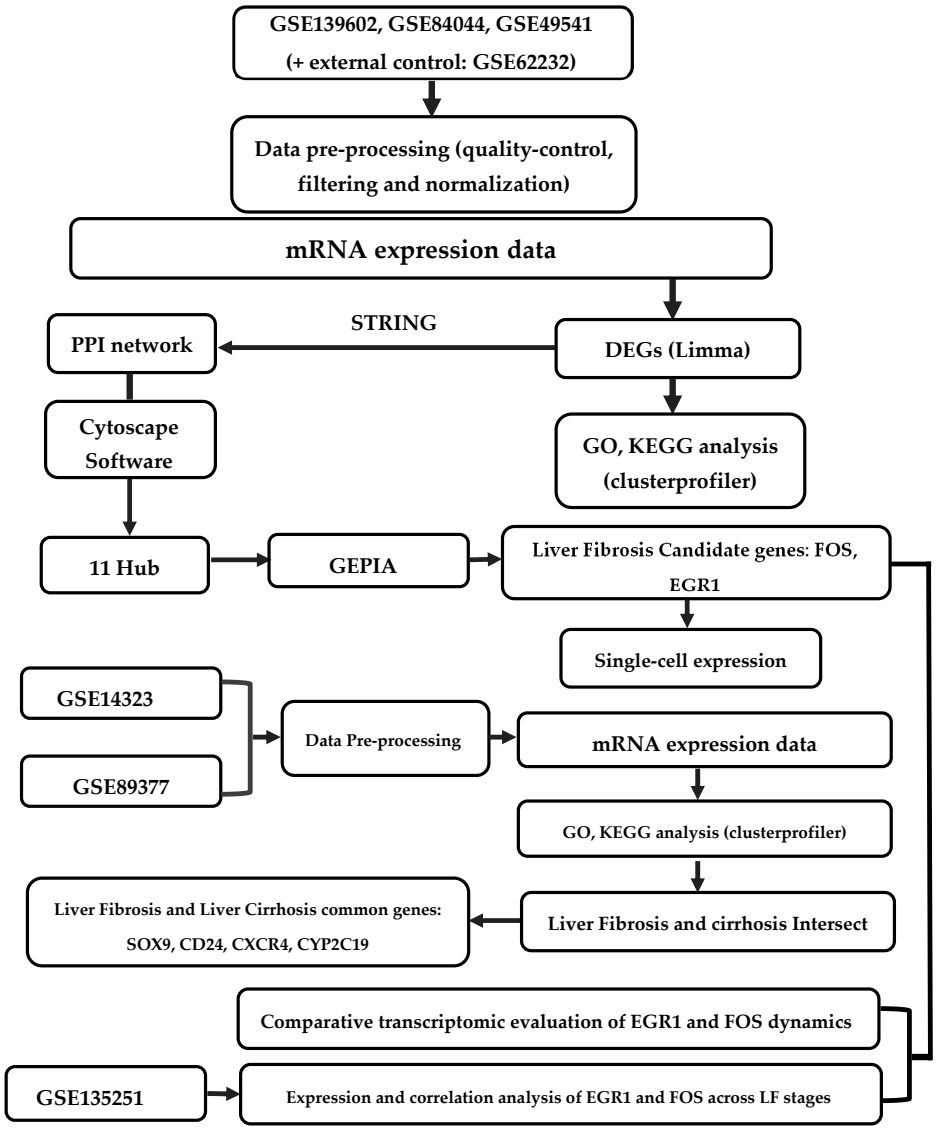


Figure 1. Workflow of our bioinformatic analysis. DEGs: differentially expressed genes, PPI: protein–protein interaction, GO: Gene Ontology, KEGG: Kyoto Encyclopedia of Genes and Genomes, GEPIA: Gene Expression Profiling Interactive Analysis.

We believe this is the first study to examine how EGR1 and FOS behave together across the different stages of liver fibrosis and whether the EGR1-FOS axis shows stage- and etiology-dependent activity. We identified 11 hub genes (MYC, FOS, CEBPB, CEBPD, DUSP1, NR3C1, NFKBIA, EGR1, MCL1, FOXO3, and CD4) and four genes shared between fibrosis and cirrhosis (SOX9, CD24, CXCR4, and CYP2C19). Notably, EGR1 exhibited dataset-dependent regulation, upregulated in GSE49541 but downregulated in GSE84044 and GSE139602, whereas FOS showed consistent downregulation. Both genes demonstrated a strong positive correlation, suggesting coregulation during hepatic fibrogenesis. Analysis via TIMER further supported EGR1's association with immune infiltration and its strong correlation with FOS in HCC. External validation using GSE135251 confirmed a significant, stage-dependent increase in both genes during fibrosis progression, underscoring their coordinated function as a dynamic regulatory axis in liver fibrogenesis.

2. Materials and Methods

2.1. Data Processing and Normalization

We used the GEO database to explore mRNA expression levels and clinical data related to LF, cirrhosis, and normal samples (accessed 20 May 2025). We downloaded the following datasets for LF: GSE139602 [9], GSE84044 [10], and GSE49541 [11]. For LC, we used GSE14323 [12] and GSE89377 [13]. All microarray datasets were imported into R for downstream analysis. The corresponding platforms were GSE139602 (GPL13667, Affymetrix Human Genome U219 Array), GSE84044 (GPL570, Affymetrix Human Genome U133 Plus 2.0 Array), GSE49541 (GPL570, Affymetrix Human Genome U133 Plus 2.0 Array), GSE14323 (GPL571, Affymetrix Human Genome U133A 2.0 Array), and GSE89377 (GPL6947, Illumina HumanHT-12 v3.0 expression beadchip). The external validation dataset GSE135251 was generated by RNA sequencing on GPL18573 (Illumina NextSeq 500). For this dataset, stage-specific analyses were performed according to the fibrosis-stage annotation available in the GEO sample metadata. Because these datasets originated from different studies, they were not merged into a single global expression matrix. Instead, each dataset was analyzed independently, considering its own platform and preprocessing status. For GSE139602, GEO provided processed Affymetrix expression values with RMA-based preprocessing. GSE49541 was analyzed as GC-RMA-processed Affymetrix data. Additionally, for the stage-based analysis of EGR1 and FOS expression, fibrosis grouping in GSE49541 was based on the original dataset metadata, in which samples were classified as mild (fibrosis stage 0–1) or advanced (fibrosis stage 3–4). GSE14323 was analyzed using the GPL571 processed Affymetrix expression matrix. From this series, only the GPL571 cirrhosis and normal liver samples relevant to the present analysis were retained, and HCC samples were excluded. GSE89377 was analyzed as a preprocessed Illumina dataset normalized by quantile normalization with GenPlex 3.0. For GSE84044 and GSE49541, internal control samples were not available for the fibrosis-versus-control comparison; therefore, control samples were obtained from the independent GEO series GSE62232 [14], generated on the same GPL570 platform, to allow for platform-matched cross-series analyses with reduced platform-related heterogeneity. Data normalization procedures are depicted in Supplementary Figure S1.

The differential expression analysis was then performed separately for each dataset using the limma package in R (Version 3.34.9), whereas DESeq2 was used for normalization and downstream analysis of the RNA-seq validation dataset GSE135251. Genes with adjusted p-value < 0.05 and $|\text{logFC}| \geq 1.0$ were considered significantly differentially expressed. Subsequently, probes were annotated using the corresponding platform annotation files. Candidate genes were identified by intersecting the independently derived DEG lists across datasets rather than through direct pooled cross-study normalization. The VennDiagram package was used to visualize common DEGs across the LF and LC datasets. Multiple linear regression was performed to assess whether the association between EGR1 and FOS persisted after adjustment for disease status. FOS was used as the dependent variable, with EGR1 and Condition (0 = control, 1 = liver fibrosis) as independent variables. Model comparison between the unadjusted and adjusted models was conducted using ANOVA.

2.2. DEGs Liver Fibrosis and Cirrhosis Intersect

In order to conduct our bioinformatic analysis, we used three transcriptomic datasets of LF and two datasets of LC from the GEO database to pinpoint the DEGs linked to LF and cirrhosis using R as software for our analysis. We found a total of 455 DEGs for LF, and for the two datasets of LC, we were able to identify 61 DEGs. Subsequently, we performed an intersection analysis, which allowed us to identify four common genes.

2.3. Gene Ontology Functional Annotation and Kyoto Encyclopedia of Genes and Genomes Pathway Analysis of DEGs for Liver Fibrosis and Cirrhosis

To investigate the biological significance of the intersected DEGs from LF and LC, specifically, Gene Ontology (GO), including the biological processes (BPs), molecular functions (MFs), cellular components (CCs), and the pathways associated with the DEGs, was identified through the Kyoto Encyclopedia of Genes and Genomes (KEGG) enrichment analysis. The clusterProfiler package was used to achieve a comprehensive set of functional annotations. An adjusted $p < 0.05$ was set as the threshold for significance.

2.4. Protein–Protein Interaction Network Analysis and Identification of Hub Genes

The Search Tool for the Retrieval of Interacting Genes (STRING) database (https://string-db.org/) was utilized to create a protein–protein interaction (PPI) network (accessed 18 June 2025). The identification of PPI relationships was possible by querying the determined intersected DEGs for LF, assessed in the STRING database, considering 0.400 as the minimum interaction score [15]. After importing the results obtained from STRING into the Cytoscape software (3.10.3), CytoHubba was used to identify hub genes by querying and ranking them by the Maximal Clique Centrality (MCC) and Edge Percolated Component (EPC).

2.5. Correlation Analysis of Hub Genes

We conducted Pearson's correlation analysis in R to examine the pairwise correlation coefficients among the expression levels of hub genes. A threshold of $p < 0.05$ was used for statistical significance.

2.6. Hub Genes Validation in GEPIA Tool

In our validation approach, we used the GEPIA (http://gepia.cancer-pku.cn) platform (accessed 8 November 2025), which combines The Cancer Genome Atlas (TCGA) and Genotype-Tissue Expression (GTEx) datasets; this allowed us to explore expression profiles, differential genes, and survival analyses [16]. For the 11 hub genes found among the DEGs related to LF, we applied the Kaplan–Meier method to assess survival to explore their influence on overall survival (OS) in liver hepatocellular carcinoma (LIHC) patients. GEPIA stratified patients into two categories, high expression and low expression, using 25% and 75% percentile values. The corresponding hazard ratios (HRs), 95% confidence intervals, and log-rank p-values were estimated, with results considered significant when $p < 0.05$ or p (HR) < 0.05.

2.7. Single-Cell Expression Landscape of EGR1 and FOS in Hepatocellular Carcinoma Microenvironment

To better characterize the cellular distribution of EGR1 and FOS within the LIHC microenvironment, we analyzed two publicly available single-cell RNA-seq datasets, GSE140228 and GSE98638, in the Tumor Immune Single-cell Hub 2 (TISCH2) database (http://tisch.comp-genomics.org) (accessed 9 November 2025). Preprocessed expression matrices and cell-type annotations, generated using Smart-seq2 and 10× Genomics platforms, were employed to assess gene-level variation across key cellular compartments, including tumor cells, macrophages, dendritic cells, and T-cell subsets. Uniform Manifold Approximation and Projection (UMAP) visualization and log-normalized data integration followed the standard TISCH2 workflow. This analysis provided a single-cell resolution map of the EGR1-FOS axis, allowing for the contextual evaluation of its cell-type-specific transcriptional activity within the immune–stromal landscape of HCC.

2.8. Tumor Infiltrating Immune Cells Analysis

The assessment of tumor-infiltrating immune cells was conducted using the TIMER database (https://cistrome.shinyapps.io/timer/), a web-based tool that provides systematic evaluations of immune cell infiltration across various cancer types using RNA-sequencing data from TCGA (accessed 12 November 2025) [17]. EGR1 and FOS expression levels and the abundance of six major immune infiltrates (B cells, CD4 + T cells, CD8 + T cells, macrophages, neutrophils, and dendritic cells) were evaluated. To examine whether genomic alterations influence immune infiltration, somatic copy number alteration (SCNA) data for EGR1 and FOS were analyzed through the TIMER SCNA module. SCNA categories were defined according to GISTIC 2.0. Infiltration levels of the same immune cell subsets were compared across these Copy Number Variation categories using a two-sided Wilcoxon rank-sum test; the results are displayed as boxplots. Statistically significant differences ($p < 0.05$) are indicated directly on the plots. Finally, the direct relationship between EGR1 and FOS expressions was explored using the Correlation module of TIMER (accessed 12 November 2025).

2.9. Comparative Transcriptomic Evaluation of EGR1-FOS Dynamics in NAFLD- and HBV-Associated Fibrosis

Publicly available transcriptomic datasets, GSE49541 (NAFLD-associated fibrosis) and GSE84044 (HBV-related fibrosis), were obtained from the GEO database to examine the expression dynamics of EGR1 and FOS across distinct fibrotic contexts. Because EGR1 showed inconsistent trends, upregulated in NAFLD samples compared to normal liver but downregulated in viral fibrosis, we further explored whether disease origin influenced its behavior. In GSE49541, we compared EGR1 and FOS expression between mild (stage 0–1) and advanced (stage 3–4) fibrosis to assess stage-dependent regulation, while in GSE84044, their expression was analyzed between normal and HBV-fibrotic liver tissues. Normalized expression data were $\log_2$-transformed and analyzed using the Wilcoxon rank-sum test in R, with visualization performed through ggplot2 and ggpubr. This approach allowed us to clarify the apparent fluctuation of EGR1, revealing its upregulation with fibrosis progression in NAFLD and its suppression in HBV-induced fibrosis, supporting a context-dependent regulatory pattern of the EGR1-FOS axis.

2.10. Analysis of EGR1 and FOS Expression and Correlation Across Liver Fibrosis Stages

To further validate the fluctuating behavior of the EGR1-FOS axis across LF progression, an independent validation was performed using the GSE135251 dataset, which profiles NAFLD-derived LF [18]. This dataset enabled stage-specific assessment of gene expression across the four fibrosis stages. Gene expression matrices were preprocessed and normalized before statistical assessment using the Robust Multi-array Average algorithm implemented in the affy package in R. Data distribution was examined using the Shapiro–Wilk test, revealing a non-normal pattern for both EGR1 and FOS, thereby warranting the use of the Mann–Whitney U test for pairwise stage comparisons. Median expression values and 95% confidence intervals were calculated to quantify differences across stages. The ggplot2 and ggpubr packages were used for visualization. Correlation analyses between EGR1 and FOS expression within each LF stage were performed using Pearson's correlation test, and regression plots were generated to illustrate stage-specific associations. Significance was set at $p < 0.05$.

3. Results

3.1. Identification of DEGs Between Liver Fibrosis, Liver Cirrhosis and Normal Liver Tissue

We used three datasets (GSE139602, GSE84044, and GSE49541) to analyze DEGs between hepatic fibrosis and normal liver tissue. In GSE139602, 105 genes displayed increased

expression, while 1084 were reduced. Examination of GSE84044 indicated 276 upregulated and 7856 downregulated genes; furthermore, the analysis of GSE49541 uncovered 29022 transcripts with elevated expression, and 601 were downregulated. In contrast, concerning LC, 589 upregulated and 162 downregulated genes were detected in GSE14323, and 75 upregulated genes, along with 34 downregulated genes, were noted in GSE89377.

To visualize the DEGs, volcano plots were generated, as shown in Figure 2a–c and heatmaps were employed to compare the transcript abundance of DEGs across datasets, as shown in Figure 2d–f. For LC, the expression trends of overlapping genes were displayed using volcano plots (Figure 3a,b) and heatmap representations (Figure 3c,d). The intersection of these results was represented in a Venn diagram in Figure 4a for LF and in Figure 4b for LC. This approach enabled us to pinpoint four core genes (SOX9, CD24, CXCR4, and CYP2C19) shared between LF and LC datasets (Figure 4c).

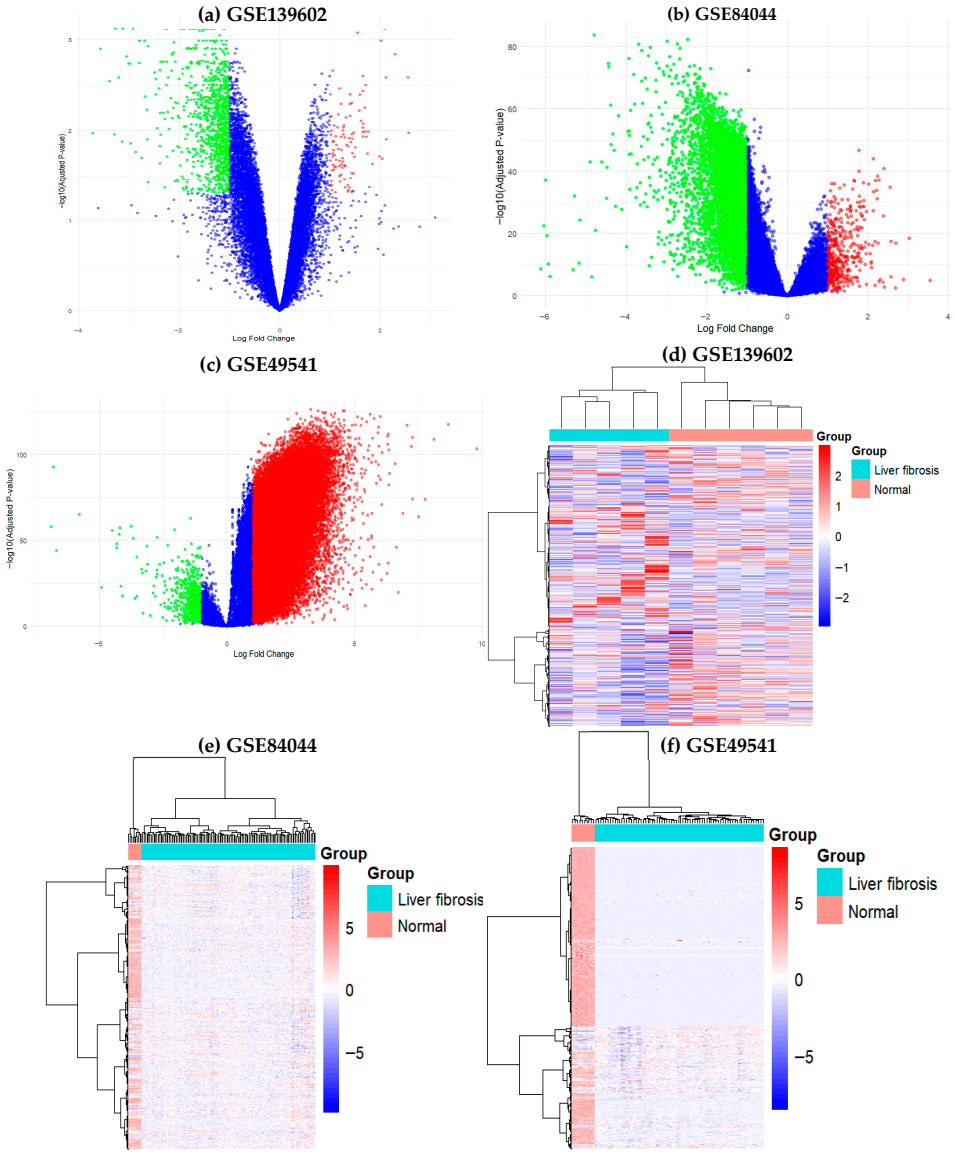


Figure 2. Identification of DEGs in liver fibrosis. (**a**–**c**) Volcano plots for datasets GSE139602, GSE84044, and GSE49541, displaying significantly upregulated (red) and downregulated (green) genes ($|\log_2 FC| \geq 1.0$, adjusted $p < 0.05$). Blue points indicate genes without significant expression changes. (**d**–**f**) Heatmaps showing hierarchical clustering of DEGs that distinguish liver fibrosis samples from normal liver tissues across the three datasets.

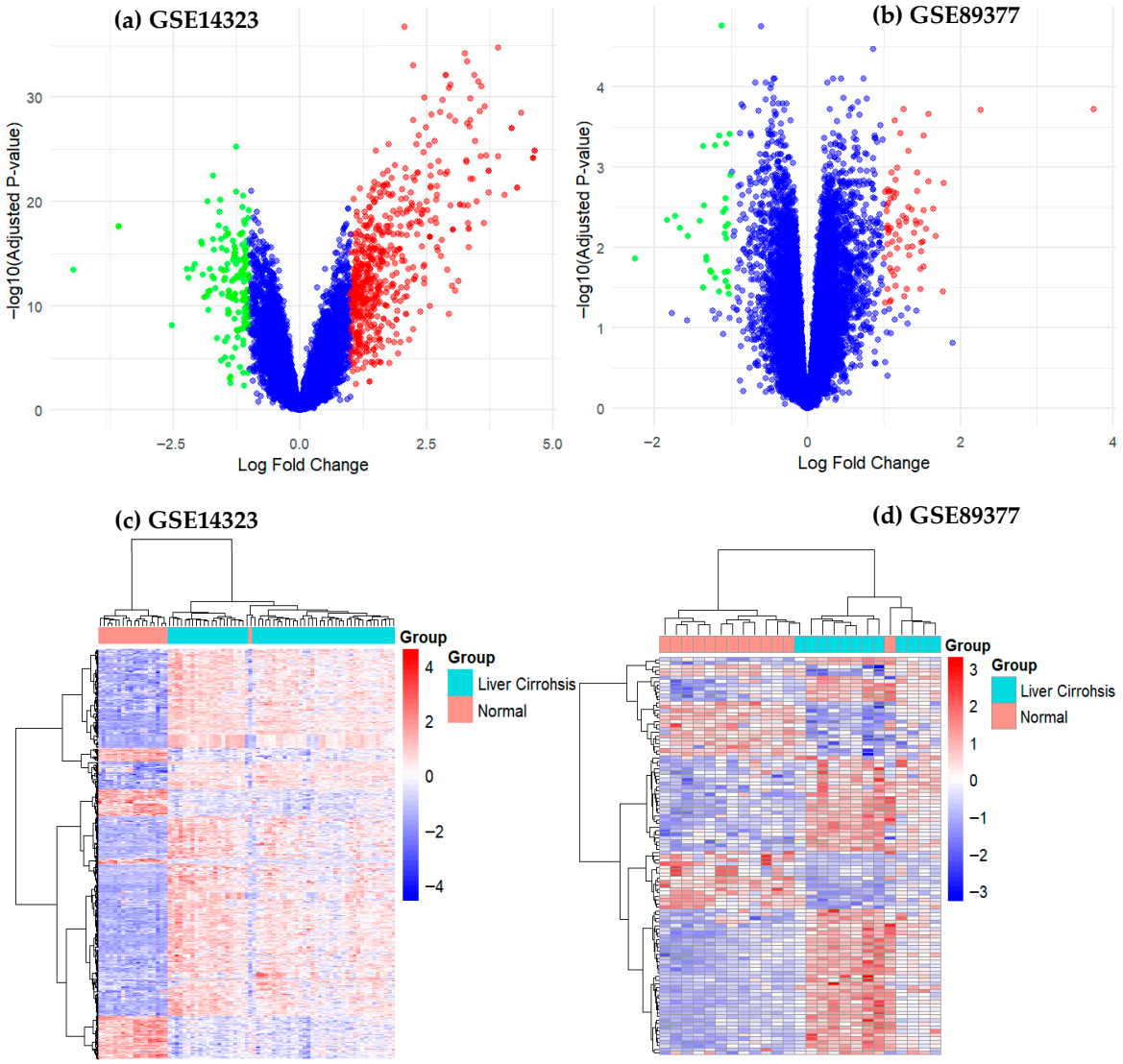


Figure 3. Identification of DEGs in liver cirrhosis. (**a**,**b**) Volcano plots corresponding to GSE14323 and GSE89377, displaying transcripts with significant upregulation (red; $|\log_2 FC| \geq 1.0$, adjusted $p < 0.05$) and downregulation (green; $|\log_2 FC| \leq -1.0$, adjusted $p < 0.05$). Blue points indicate genes showing no statistically meaningful expression variation. (**c**) and (**d**) represent hierarchical clustering analysis of DEGs between liver fibrosis and normal tissues in GSE14323 and GSE89377, respectively.

3.2. Functional Enrichment Analysis of DEGs Intersect

To elucidate biological functions, the total DEG intersection of the three datasets in LF was used in the GO analysis, and the results are shown in Figure 5a–c and Table 1. The criteria were adjusted to $p < 0.05$. GO analysis indicated a significant enrichment in BP associated with positive regulation of DNA-templated transcription (FDR = 0.0116), the fibroblast growth factor receptor signaling pathway (FDR = 0.0116), cellular response to tumor necrosis factor (FDR = 0.0116), the insulin-like growth factor receptor signaling pathway (FDR = 0.0305), and the platelet-derived growth factor receptor-alpha signaling pathway (FDR = 0.0306). The CCs of the DEGs were enriched in the cytoplasm (FDR = 1.6348×10^{-8}), nucleoplasm (FDR = 3.1055×10^{-8}), nucleus (FDR = 4.6676×10^{-5}), cytoplasmic stress granule (FDR = 0.0256), and chromatin (FDR = 0.0296). Functional enrichment analysis of the MF category revealed a strong overrepresentation of terms associated with protein binding (FDR = 1.2494×10^{-15}), protein tyrosine kinase collagen receptor activity (FDR = 0.0075), platelet-derived growth factor alpha-receptor activity (FDR = 0.0075), macrophage colony-stimulating factor re-

ceptor activity (FDR = 0.0075), insulin receptor activity (FDR = 0.0075) and insulin-like growth factor receptor activity (FDR = 0.0080), the KEGG pathway analysis was not significant for LF. Furthermore, the total DEGs intersection in LC was used for GO analysis (Figure 6 and Table 2). GO analysis revealed enrichment in BP related to immune response (FDR = 0.0003), the chemokine-mediated signaling pathway (FDR = 0.0007), positive regulation of cell migration (FDR = 0.0028), and positive regulation of phosphatidylinositol 3-kinase/protein kinase B signal transduction (FDR = 0.0159). In addition, the CCs of DEGs revealed enrichment in the extracellular region (FDR = 2.3119×10^{-9}), extracellular space (FDR = 3.3909×10^{-9}), collagen-containing extracellular matrix (FDR = 6.5224×10^{-6}), and extracellular exosome (FDR = 0.014). Molecular function analysis elucidated a significant enrichment in MF associated with extracellular matrix structural constituents (FDR = 1.7290×10^{-5}) and chemokine activity (FDR = 5.1632×10^{-5}). According to the KEGG pathway enrichment, the analyzed genes are mainly involved in the chemokine signaling pathway (FDR = 0.0105) and cytokine–cytokine receptor interaction (FDR = 0.0110).

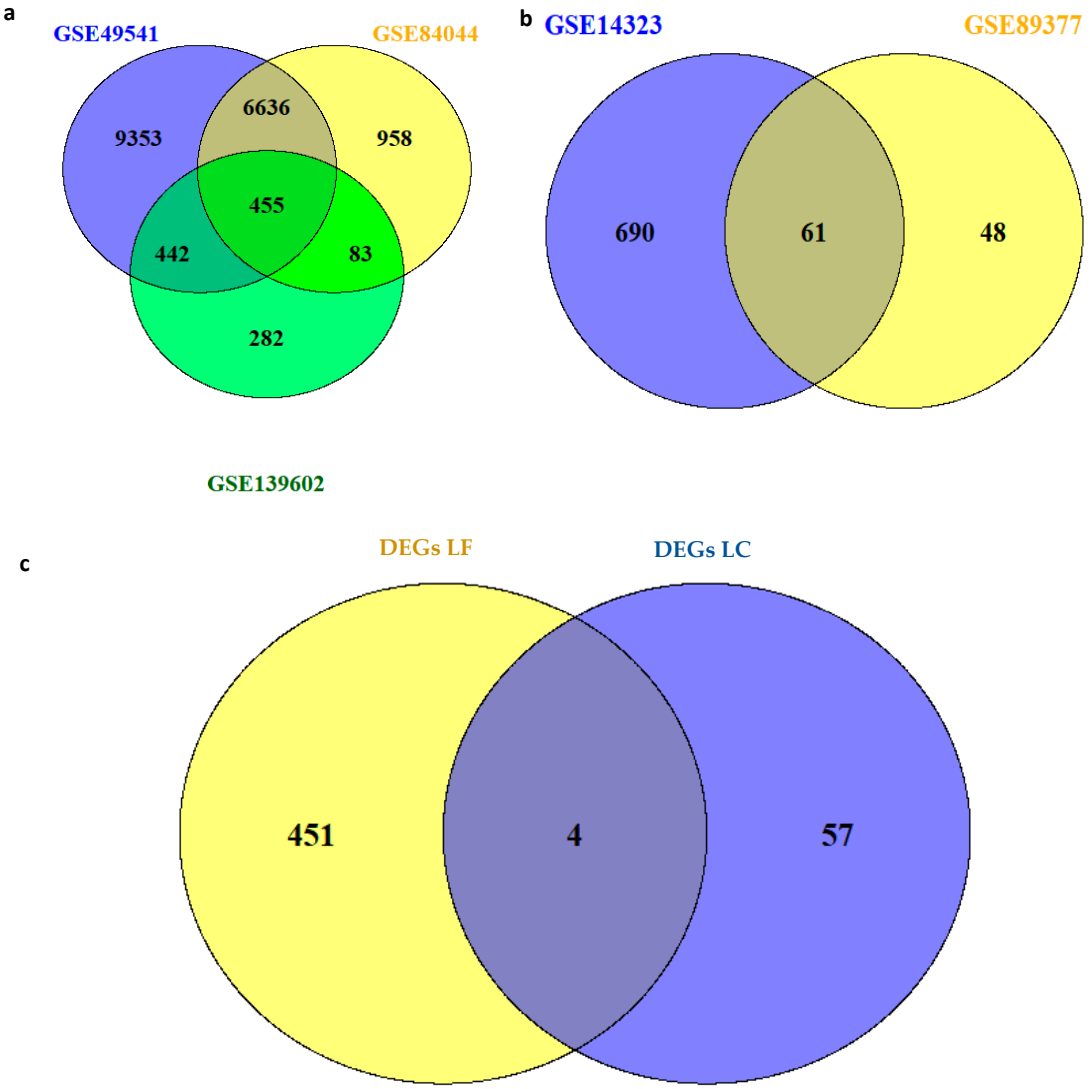


Figure 4. Venn diagrams. (**a**) Venn diagram of all DEGs intersected (n = 455) in liver fibrosis relative to normal liver tissue in the three GEO datasets. (**b**) Venn diagram of all DEGs intersected (n = 61) in liver cirrhosis relative to normal liver tissue in the three GEO datasets. (**c**) Venn diagram of intersecting genes between liver fibrosis and liver cirrhosis in the five analyzed GEO datasets.

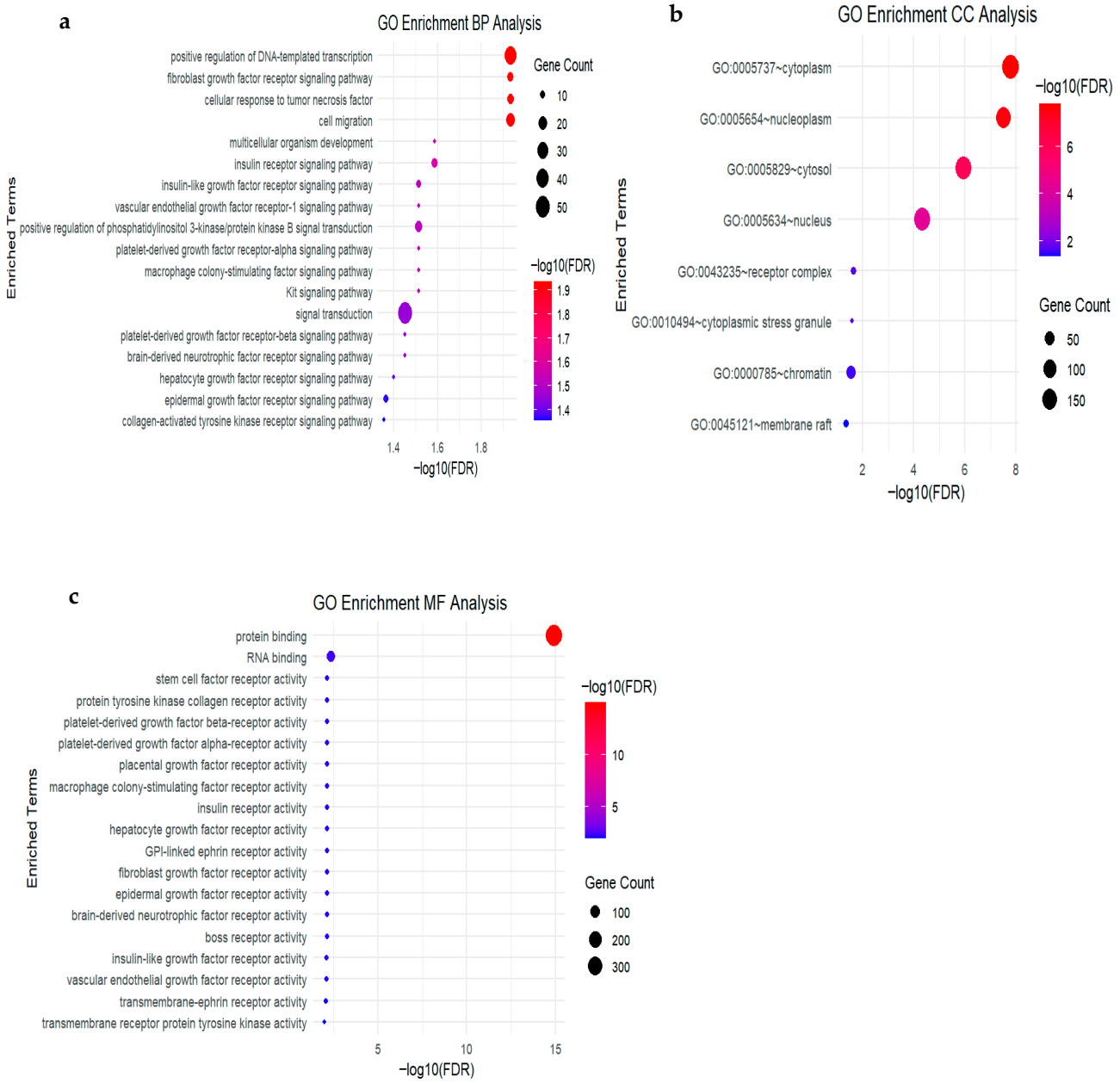


Figure 5. GO enrichment results (p adjust < 0.05). (**a**) Key biological processes associated with the DEGs. (**b**) Key cellular components associated with the DEGs. (**c**) Key molecular functions associated with the DEGs in liver fibrosis.

Table 1. The results of GO. Biological processes (BPs), cellular components (CCs), and molecular functions (MFs) for liver fibrosis, considering p-adjusted < 0.05.

Category	ID	Description	Count	FDR
BP	GO:0071356	cellular response to tumor necrosis factor	13	0.0116655449654847
	GO:0045893	positive regulation of DNA-templated transcription	36	0.0116655449654847
	GO:0016477	cell migration	20	0.0116655449654847
	GO:0008543	fibroblast growth factor receptor signaling pathway	12	0.0116655449654847
	GO:0007275	multicellular organism development	8	0.0259521508368659
	GO:0008286	insulin receptor signaling pathway	12	0.0259521508368659
	GO:0048009	insulin-like growth factor receptor signaling pathway	10	0.0305381189858401

Table 1. *Cont.*

Category	ID	Description	Count	FDR
	GO:0036323	vascular endothelial growth factor receptor-1 signaling pathway	8	0.0306137989648556
	GO:0035790	platelet-derived growth factor receptor-alpha signaling pathway	8	0.0306137989648556
	GO:0038145	macrophage colony-stimulating factor signaling pathway	8	0.0306137989648556
	GO:0038109	Kit signaling pathway	8	0.0306137989648556
	GO:0051897	positive regulation of phosphatidylinositol 3-kinase/protein kinase B signal transduction	15	0.0306137989648556
	GO:0035791	platelet-derived growth factor receptor-beta signaling pathway	8	0.0352758650651886
	GO:0031547	brain-derived neurotrophic factor receptor signaling pathway	8	0.0352758650651886
	GO:0007165	signal transduction	51	0.0352758650651886
	GO:0048012	hepatocyte growth factor receptor signaling pathway	8	0.0396872029609826
	GO:0007173	epidermal growth factor receptor signaling pathway	10	0.0430336165183487
	GO:0038063	collagen-activated tyrosine kinase receptor signaling pathway	8	0.0440175452919444
CC	GO:0005737	cytoplasm	192	$1.63483943113957 \times 10^{-8}$
	GO:0005654	nucleoplasm	143	$3.10550668445599 \times 10^{-8}$
	GO:0005829	cytosol	176	$1.12101570577927 \times 10^{-6}$
	GO:0005634	nucleus	182	$4.66763811131671 \times 10^{-5}$
	GO:0043235	receptor complex	15	0.0239662873412864
	GO:0010494	cytoplasmic stress granule	10	0.0256660075722775
	GO:0000785	chromatin	43	0.0296010248658772
	GO:0045121	membrane raft	14	0.0452357122579773
MF	GO:0005515	protein binding	392	1.2494×10^{-15}
	GO:0003723	RNA binding	61	0.0045
	GO:0005011	macrophage colony-stimulating factor receptor activity	8	0.0075
	GO:0005020	stem cell factor receptor activity	8	0.0075
	GO:0038062	protein tyrosine kinase collagen receptor activity	8	0.0075
	GO:0036332	placental growth factor receptor activity	8	0.0075
	GO:0005004	GPI-linked ephrin receptor activity	8	0.0075
	GO:0060175	brain-derived neurotrophic factor receptor activity	8	0.0075
	GO:0005009	insulin receptor activity	8	0.0075
	GO:0005018	platelet-derived growth factor alpha-receptor activity	8	0.0075
	GO:0008288	boss receptor activity	8	0.0075
	GO:0005019	platelet-derived growth factor beta-receptor activity	8	0.0075
	GO:0005008	hepatocyte growth factor receptor activity	8	0.0075
	GO:0005007	fibroblast growth factor receptor activity	8	0.0075
	GO:0005006	epidermal growth factor receptor activity	8	0.0075
	GO:0005010	insulin-like growth factor receptor activity	8	0.0080
	GO:0005021	vascular endothelial growth factor receptor activity	8	0.0085
	GO:0005005	transmembrane-ephrin receptor activity	8	0.0091
	GO:0004714	transmembrane receptor protein tyrosine kinase activity	7	0.0105

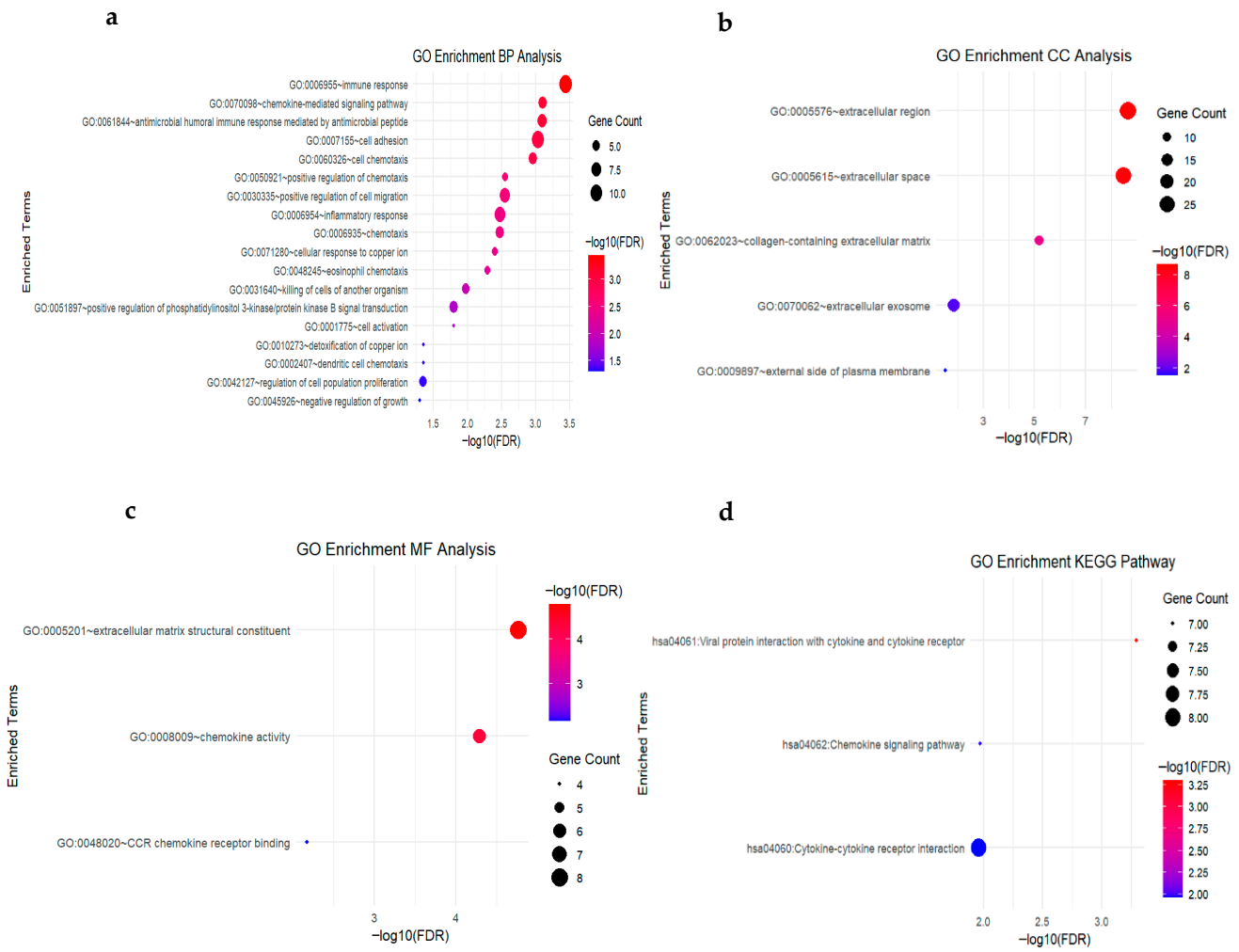


Figure 6. GO enrichment and KEGG pathway analysis results (adjusted *p*-value < 0.05). (**a**) Key biological processes associated with the DEGs. (**b**) Key cellular components associated with the DEGs. (**c**) Key molecular functions associated with the DEGs. (**d**) Key KEGG pathways associated with the DEGs in liver cirrhosis.

Table 2. The results of GO. Biological processes (BP), cellular components (CC)and molecular functions (MF) and KEGG pathway analysis for liver cirrhosis, considering *p*-adjusted < 0.05.

Category	ID	Description	Count	FDR
BP	GO:0006955	immune response	12	0.0003
	GO:0070098	chemokine-mediated signaling pathway	6	0.0007
	GO:0061844	antimicrobial humoral immune response mediated by antimicrobial peptide	7	0.0007
	GO:0007155	cell adhesion	11	0.0009
	GO:0060326	cell chemotaxis	6	0.0011
	GO:0030335	positive regulation of cell migration	8	0.0028
	GO:0050921	positive regulation of chemotaxis	4	0.0028
	GO:0006954	inflammatory response	9	0.0033
	GO:0006935	chemotaxis	6	0.0033
	GO:0071280	cellular response to copper ion	4	0.0039
	GO:0048245	eosinophil chemotaxis	4	0.0050
	GO:0031640	killing of cells of another organism	5	0.0105
	GO:0001775	cell activation	3	0.0159
	GO:0051897	positive regulation of phosphatidylinositol 3-kinase/protein kinase B signal transduction	6	0.0159

Table 2. *Cont.*

Category	ID	Description	Count	FDR
	GO:0002407	dendritic cell chemotaxis	3	0.0441
	GO:0010273	detoxification of copper ion	3	0.0441
	GO:0042127	regulation of cell population proliferation	5	0.0451
	GO:0045926	negative regulation of growth	3	0.0497
CC	GO:0005576	extracellular region	28	2.3119×10^{-9}
	GO:0005615	extracellular space	26	3.3909×10^{-9}
	GO:0062023	collagen-containing extracellular matrix	11	6.5224×10^{-6}
	GO:0070062	extracellular exosome	17	0.0142
	GO:0009897	external side of plasma membrane	7	0.0302
MF	GO:0005201	extracellular matrix structural constituent	8	1.7290×10^{-5}
	GO:0008009	chemokine activity	6	5.1632×10^{-5}
	GO:0048020	CCR chemokine receptor binding	4	0.0067
KEGG Pathway Analysis	hsa04061	viral protein interaction with cytokine and cytokine receptor	7	0.0005
	hsa04062	chemokine signaling pathway	7	0.0105
	hsa04060	cytokine–cytokine receptor interaction	8	0.0110

3.3. PPI Network Construction and Identification of Hub Genes

To identify the main regulatory genes involved in LF, a PPI network was constructed using 455 DEGs. The resulting network comprised 453 nodes connected through 1365 interaction edges. PPI analysis was conducted on the top 15 identified and ranked genes using CytoHubba in Cytoscape, using two algorithms: MCC, as shown in Figure 7a and Table 3, and EPC, as shown in Figure 7b and Table 4. Eleven hub genes were identified: MYC, FOS, CEBPB, CEBPD, DUSP1, NR3C1, NFKBIA, EGR1, MCL1, FOXO3 and CD4, highlighting their significant interconnectivity, suggesting their potential implication in LF. These 11 genes were the most common interacting hub genes among the ranking algorithms and were subsequently subjected to enrichment analysis, as shown in Figure 8.

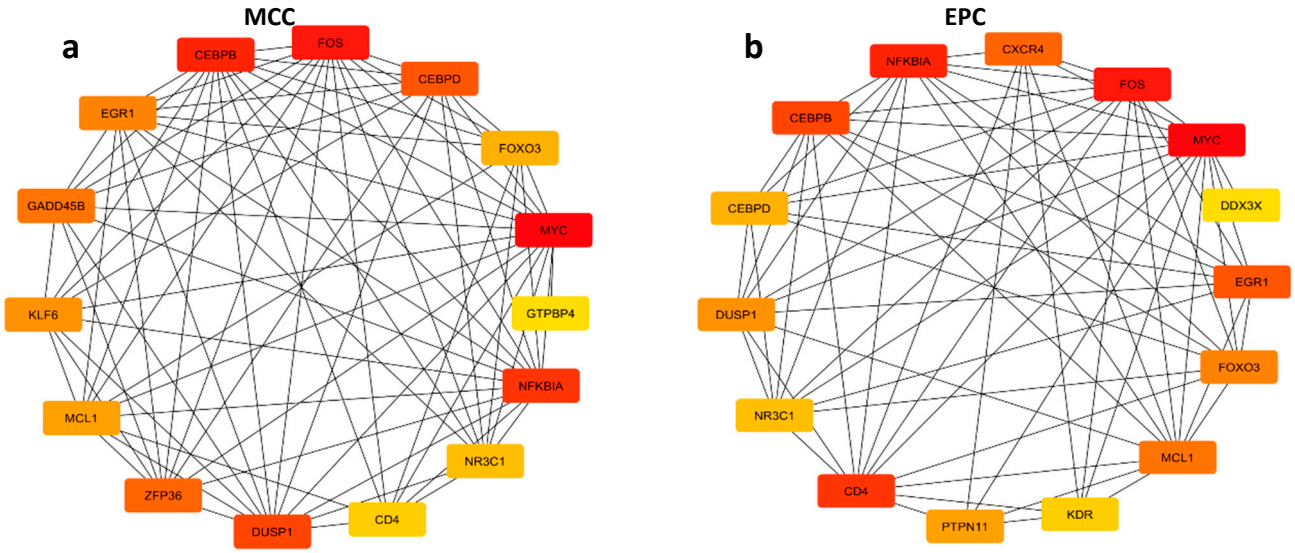


Figure 7. Protein–protein interaction network of the top 15 hub genes, generated through the STRING database and visualized using Cytoscape. Key hub genes were prioritized using the CytoHubba plugin based on the MCC and EPC ranking algorithms. (**a**) The top 15 hub genes identified using the MCC algorithm. (**b**) The top 15 hub genes determined using the EPC method.

Table 3. Top 15 hub genes in PPI network module 2 ranked by MCC method in CytoHubba.

Rank	Gene Symbol	Description	Score
1	MYC	v-myc avian myelocytomatosis viral oncogene homolog	118,597.0
2	FOS	FBJ murine osteosarcoma viral oncogene homolog	116,537.0
3	CEBPB	CCAAT/enhancer binding protein (C/EBP), beta	112,240.0
4	NFKBIA	nuclear factor of kappa light polypeptide gene enhancer in B-cells inhibitor, alpha	111,724.0
5	DUSP1	dual-specificity phosphatase 1	99,531.0
6	CEBPD	CCAAT/enhancer binding protein (C/EBP), delta	92,506.0
7	ZFP36	ZFP36 ring finger protein	90,888.0
8	GADD45B	growth arrest and DNA-damage-inducible, beta	80,808.0
9	EGR1	early growth response 1	58,169.0
10	KLF6	Kruppel-like factor 6	45,393.0
11	MCL1	myeloid cell leukemia 1	20,238.0
12	FOXO3	forkhead box O3	13,489.0
13	NR3C1	nuclear receptor subfamily 3, group C, member 1 (glucocorticoid receptor)	12,470.0
14	CD4	CD4 molecule	12,203.0
15	GTPBP4	GTP-binding protein 4	12,153.0

Table 4. Top 15 hub genes in PPI network module 2 ranked by EPC method in CytoHubba.

Rank	Gene Symbol	Description	Score
1	MYC	v-myc avian myelocytomatosis viral oncogene homolog	73.11599999999996
2	FOS	FBJ murine osteosarcoma viral oncogene homolog	69.48600000000006
3	NFKBIA	nuclear factor of kappa light polypeptide gene enhancer in B-cells inhibitor, alpha	65.35400000000011
4	CD4	CD4 molecule	64.94000000000011
5	CEBPB	CCAAT/enhancer binding protein (C/EBP), delta	60.24800000000016
6	EGR1	early growth response 1	58.80100000000011
7	CXCR4	chemokine (C-X-C motif) receptor 4	57.98200000000006
8	MCL1	myeloid cell leukemia 1	57.723000000000106
9	FOXO3	forkhead box O3	57.423000000000044
10	DUSP1	dual-specificity phosphatase 1	56.067000000000085
11	PTPN11	protein tyrosine phosphatase, non-receptor type 11	55.55200000000014
12	CEBPD	CCAAT/enhancer binding protein (C/EBP), delta	54.643000000000114
13	NR3C1	nuclear receptor subfamily 3, group C, member 1 (glucocorticoid receptor)	54.154000000000025
14	KDR	kinase insert domain receptor	52.15900000000013
15	DDX3X	DEAD (Asp-Glu-Ala-Asp) box helicase 3, X-linked	51.16100000000017

3.4. Hub Gene Correlation Analysis

We conducted Pearson's correlation analysis to assess co-expression dynamics among the 11 hub genes (MYC, FOS, CEBPB, NFKBIA, DUSP1, CEBPD, EGR1, MCL1, FOXO3, NR3C1, and CD4). As shown in Figure 9, EGR1 and FOS showed the highest correlation (r = 0.77), highlighting their potential implications in LF. In addition, another significant correlation was found between DUSP1 and EGR1 (r = 0.63), indicating their probable role in the inflammatory process. Furthermore, a moderate correlation was observed between MCL1 and FOS (r = 0.47), highlighting their potential implication in fibrotic remodeling and apoptosis. In addition, other moderate correlations were found between NFKBIA and DUSP1 (r = 0.45) and FOS (r = 0.46), respectively.

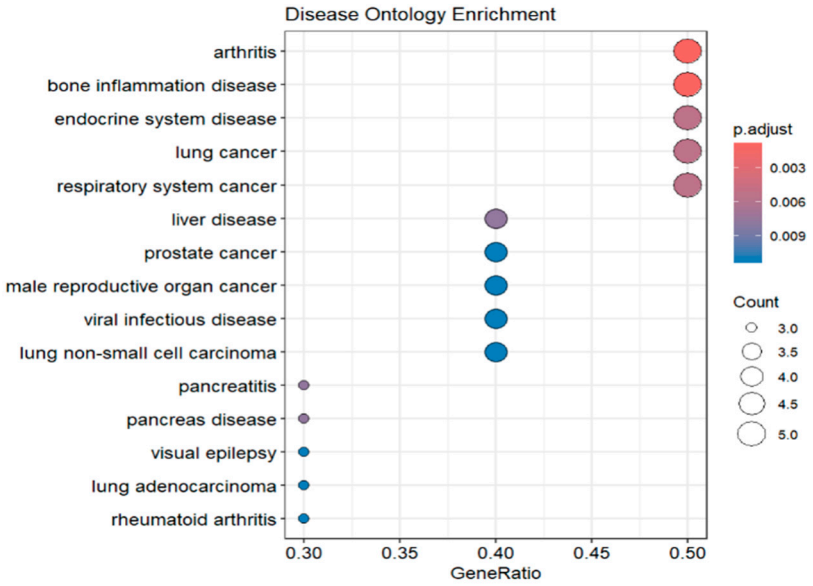


Figure 8. Disease Ontology enrichment analysis of the hub genes.

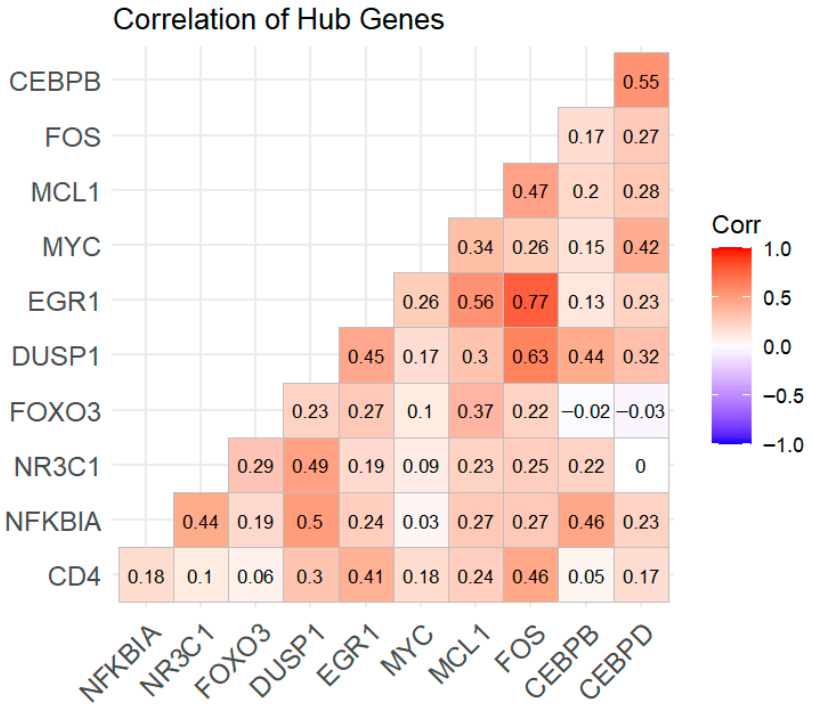


Figure 9. Correlation heatmap depicting pairwise associations among the 11 identified hub genes in liver fibrosis. Red color gradients indicate strong positive correlations (values approaching 1), whereas blue tones denote negative correlations (values approaching −1).

3.5. Hub Gene Expression and Overall Survival Analysis in LIHC Using GEPIA

GEPIA-based survival analysis was performed to examine the association between the 11 hub genes and overall survival in LIHC. Among them, EGR1 and FOS displayed differential expression (Figure 10a,b) but showed no significant association with patient survival (log-rank $p > 0.05$; Figure 10c,d). The other hub genes also lacked prognostic significance. These findings indicate that, although transcriptionally altered during hepatic fibrosis and HCC progression, EGR1 and FOS expression alone may not predict overall survival.

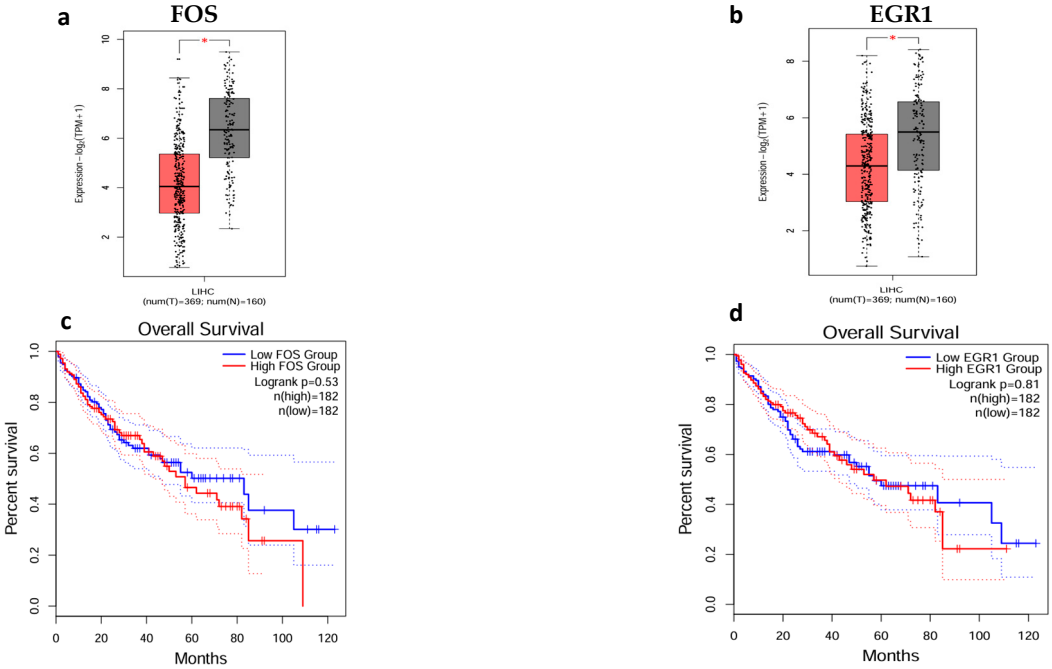


Figure 10. (**a**,**b**) Comparison of FOS and EGR1 expression between liver hepatocellular carcinoma (LIHC) and normal liver samples based on TCGA and GTEx data. Expression values are shown as $\log_2(\text{TPM} + 1)$. A red asterisk (*) denotes a statistically significant difference ($p < 0.05$) between tumor (T) and normal (N) groups. (**a**,**b**) Expression distribution of FOS and EGR1. (**c**,**d**) Kaplan–Meier survival analysis of the two significant hub genes (FOS and EGR1) in liver hepatocellular carcinoma using the GEPIA platform. Patients were stratified into high- and low-expression groups based on median thresholds, and survival outcomes were compared using log-rank tests. Survival curves for FOS and EGR1 are presented as well.

3.6. Integrated Analysis of EGR1 and FOS Expression, Copy Number Variation, and Immune Infiltration in LIHC

To elucidate the potential immunological involvement and functions of EGR1 and FOS in LIHC, we performed a comprehensive analysis using the TIMER database, integrating immune infiltration, SCNA, and gene correlation data. Both EGR1 and FOS expression were found to be positively associated with macrophage and dendritic cell infiltration, with EGR1 showing moderate correlations (macrophage: r = 0.271, $p = 5.2 \times 10^{-5}$; dendritic cells: r = 0.175, $p = 1.2 \times 10^{-3}$), and FOS displaying similar patterns (macrophage: r = 0.285, $p = 8.4 \times 10^{-8}$; dendritic cells: r = 0.216, $p = 5.7 \times 10^{-5}$). These results suggest that both transcription factors may contribute to shaping the myeloid cell landscape within the tumor microenvironment. The weak correlation of both genes with tumor purity further supports the idea that their expression is largely influenced by immune and stromal components rather than by tumor cells alone (Figure 11a).

The copy-number variation analysis showed that changes in EGR1 dosage influence the immune microenvironment in LIHC. Arm-level deletions did not significantly alter the infiltration of any immune cell type, as all corresponding *p*-values were above the significance threshold. Instead, reductions in $CD4^+$ T-cell, macrophage, neutrophil, and dendritic-cell infiltration were observed mainly in tumors carrying EGR1 gains or high-level amplifications, indicating that excessive EGR1 copy number may dampen immune recruitment. $CD8^+$ T cells were largely unaffected across all SCNA categories. In contrast, FOS SCNA categories did not show statistically significant effects on immune infiltration, implying that its immune-related activity is primarily driven by transcriptional regulation rather than genomic variation (Figure 11b).

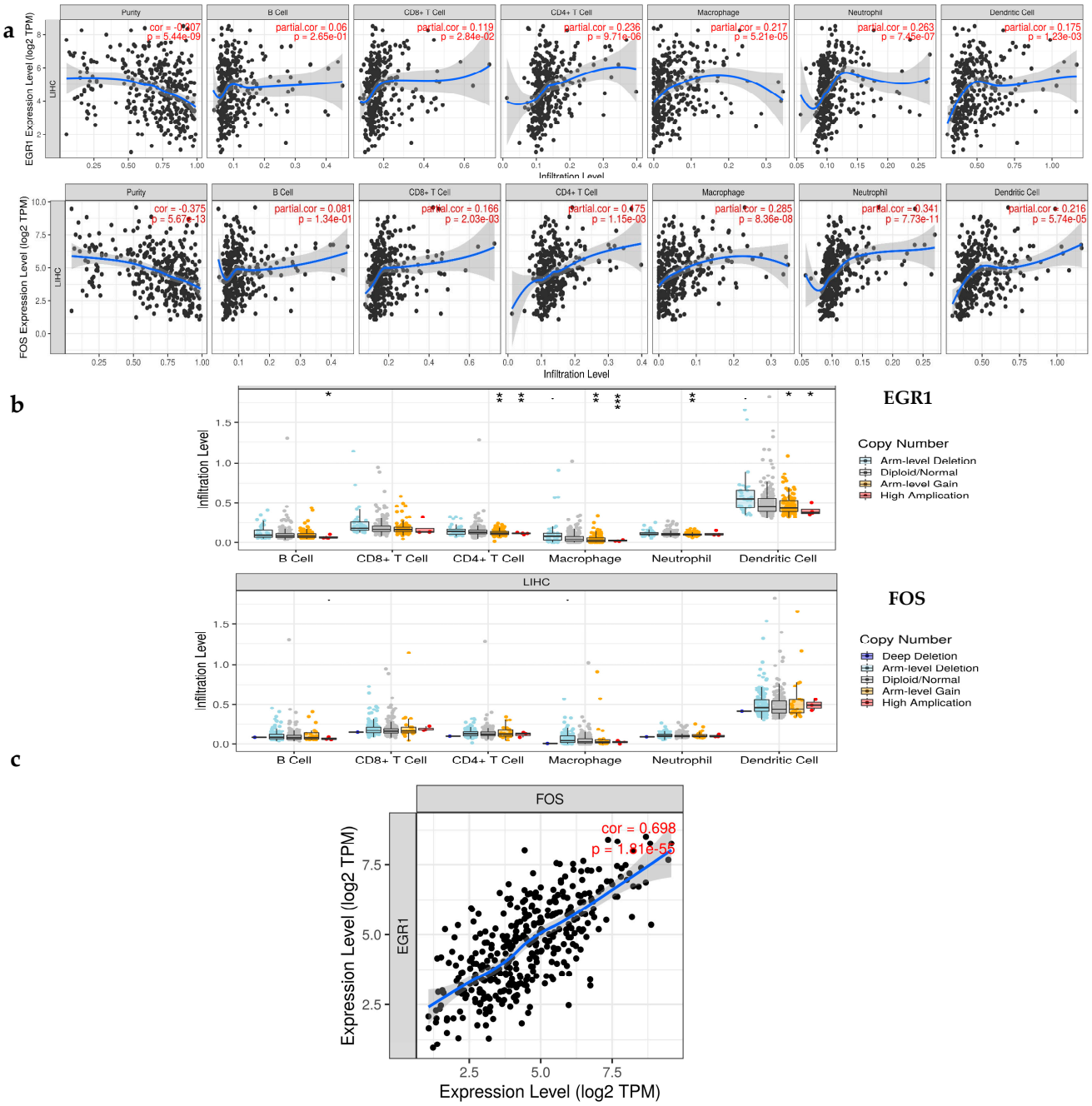


Figure 11. Immune infiltration, copy number variation, and expression correlation analyses of EGR1 and FOS in liver hepatocellular carcinoma (LIHC). (**a**) Scatter plots showing the correlations between EGR1 and FOS expression levels and the infiltration of six immune cell types (B Cell, CD8+ T Cell, CD4+ T Cell, Macrophage, Neutrophil and Dendritic Cell) in LIHC. (**b**) Boxplots showing immune cell infiltration levels in LIHC samples with different EGR1 and FOS somatic copy number alteration (SCNA) categories. (**c**) Correlation between EGR1 and FOS expression levels in LIHC based on Spearman's analysis. Statistical significance is indicated as follows: * $p < 0.05$; ** $p < 0.01$; *** $p < 0.001$.

Finally, a strong positive correlation was observed between EGR1 and FOS mRNA expression levels (Spearman's r = 0.698, $p = 1.81 \times 10^{-55}$) (Figure 11c), suggesting a coordinated activation pattern between these immediate-early transcription factors. This co-expression supports the existence of an EGR1-FOS axis potentially orchestrating downstream transcriptional programs involved in inflammation and immune modulation. Collectively, these findings identify EGR1 as a genomically sensitive modulator of immune

infiltration and highlight a possible synergistic role for EGR1 and FOS in orchestrating immune responses within the HCC microenvironment.

3.7. Single-Cell Distribution of EGR1 and FOS in the HCC Microenvironment

Single-cell RNA-seq analysis of LIHC datasets LIHC_GSE140228 and LIHC_GSE98638 revealed that both EGR1 and FOS display a low-to-moderate but structured expression pattern across the tumor microenvironment. In both datasets, transcripts were mainly detected within proliferative tumor cells, macrophages, and activated T-cell subsets, whereas stromal and quiescent immune cells showed minimal expression. UMAPs demonstrated partially overlapping expression domains for EGR1 and FOS, suggesting their potential coregulation in stress-activated and proliferative cell populations. Although neither gene was broadly expressed across all malignant clusters, their enrichment in immune-interacting niches supports a context-dependent activation of the EGR1-FOS axis in the inflammatory and regenerative processes associated with fibrosis-linked hepatocarcinogenesis (Figure 12).

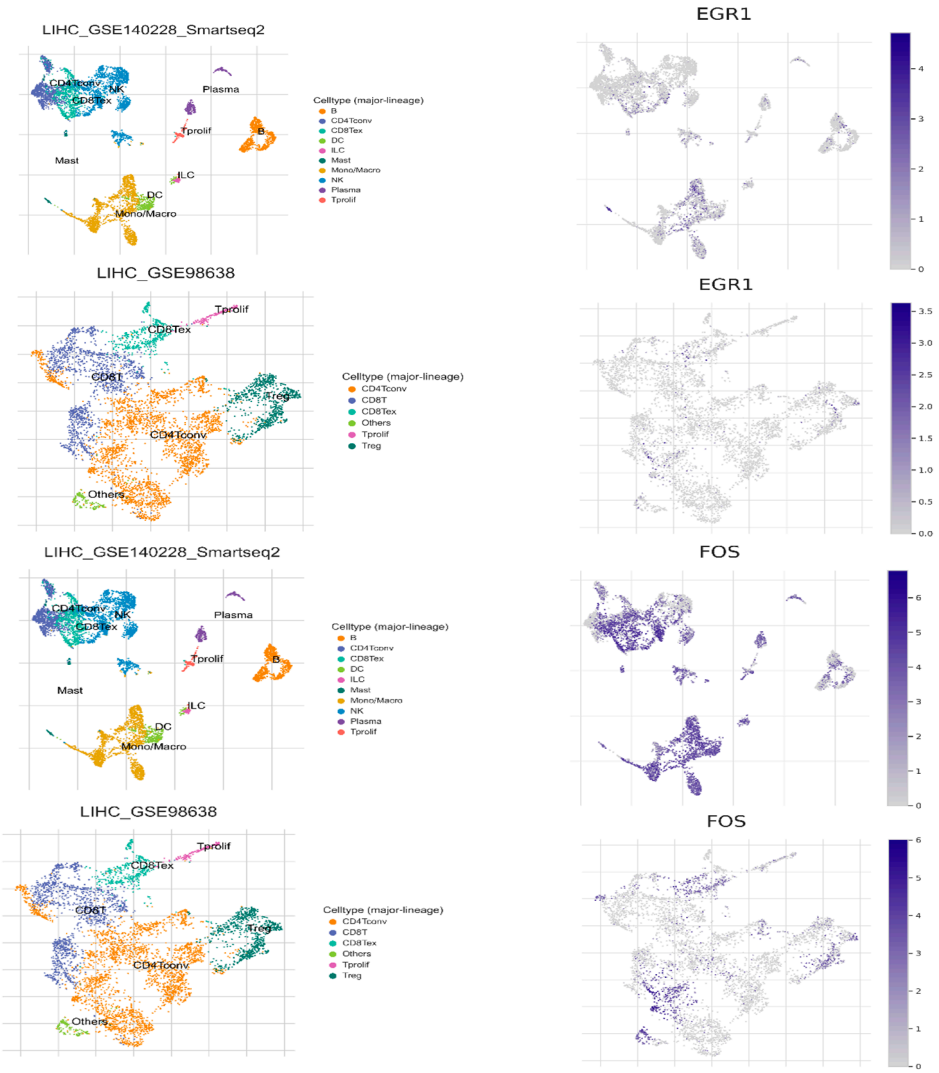


Figure 12. Uniform Manifold Approximation and Projection (UMAP) plots showing the expression and distribution patterns of EGR1 and FOS across distinct cell populations in two liver single-cell RNA sequencing datasets (LIHC_GSE140228_SmartSeq2 and LIHC_GSE98638). Cell clusters are annotated according to major immune and stromal lineages, including $CD4^+$ T cells, $CD8^+$ T cells, NK cells, macrophages/monocytes, B cells, plasma cells, mast cells, endothelial cells, and proliferating cells.

3.8. Comparative Analysis of the EGR1-FOS Axis in NAFLD and HBV-Associated Liver Fibrosis

In the NAFLD-associated fibrosis dataset (GSE49541), analysis revealed a significant increase in EGR1 expression in advanced fibrosis stages (3–4) compared with mild stages (0–1) ($p = 0.0047$), while FOS expression showed no significant change ($p = 0.4676$). Conversely, in the HBV-related fibrosis dataset (GSE84044), both EGR1 and FOS were markedly downregulated in HBV-fibrotic liver tissues compared with normal samples ($p = 4.93 \times 10^{-6}$ and $p = 1.79 \times 10^{-7}$, respectively). These results show a difference in the expression patterns of EGR1 and FOS in NAFLD-associated fibrosis and in viral-origin fibrosis (HBV-LF) (Figure 13).

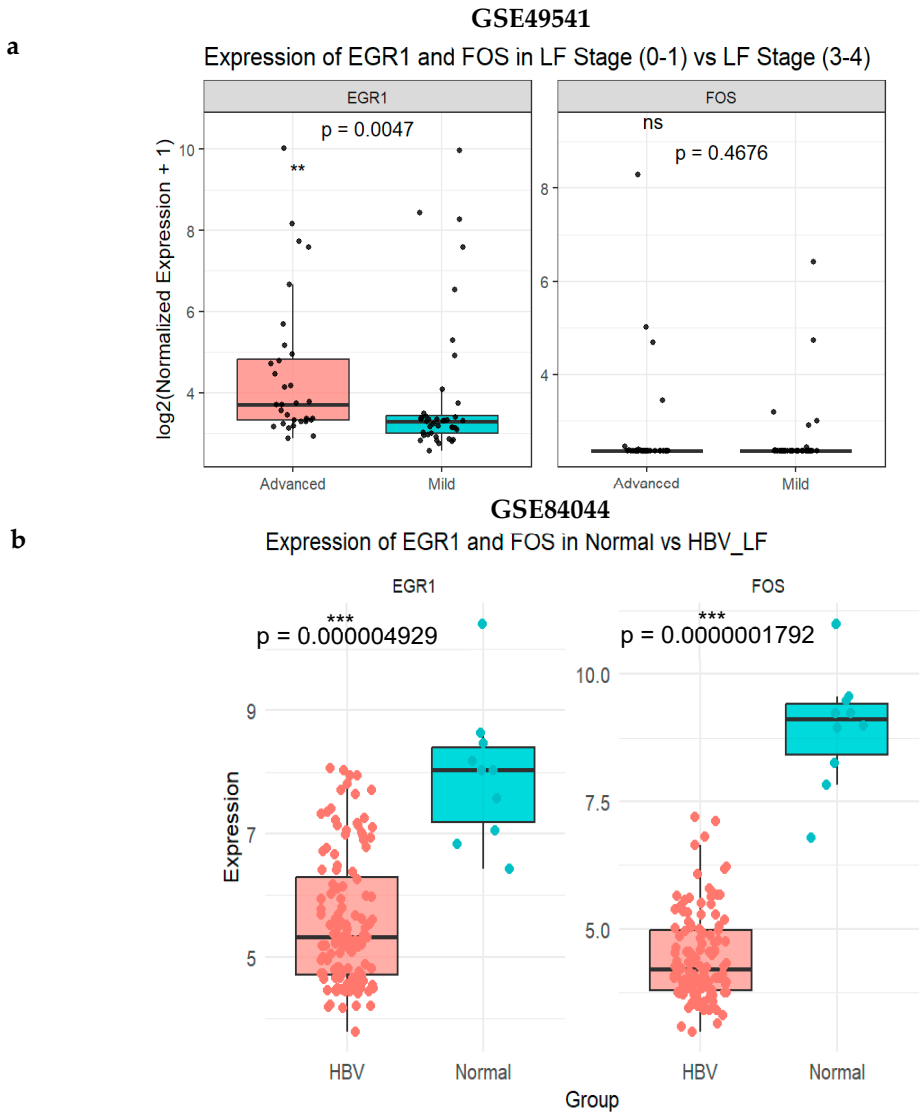


Figure 13. Differential expressions of EGR1 and FOS in liver fibrosis progression of distinct etiologies. (**a**) Boxplots show the normalized expression levels of EGR1 and FOS in liver fibrosis samples from the GSE49541 dataset, comparing advanced fibrosis stages (3–4) to early stages (0–1) in NAFLD-origin liver fibrosis. (**b**) Analysis of the GSE84044 dataset compares gene expression in normal liver samples vs. HBV-associated liver fibrosis (HBV_LF). Statistical significance is indicated as follows: ** $p < 0.01$; *** $p < 0.001$.

3.9. Stage-Specific Expression and Correlation Dynamics of the EGR1-FOS Axis in Liver Fibrosis

Analysis of the external validation dataset revealed a significant increase in EGR1 expression from early to advanced stages of LF, with marked differences between stages 1 vs. 3 ($p = 0.0008$) and stages 1 vs. 4 ($p = 0.0035$). Similarly, FOS expression progressively increased with fibrosis severity, showing significant upregulation at stages 3 ($p = 0.0001$) and 4 ($p = 0.0188$) compared to stage 1, as shown in Figure 14a and Table 5. Correlation analyses demonstrated a

strong positive association between EGR1 and FOS across all stages (R = 0.79–0.95, $p < 0.001$), with the highest correlation observed in stage 4 (R = 0.95, $p = 1.6 \times 10^{-7}$) (Figure 14b). In addition to correlation analysis, multiple linear regression was performed to test whether the association between EGR1 and FOS remained significant after adjustment for disease status. In the unadjusted model, EGR1 was strongly associated with FOS (β = 1.2053, SE = 0.0892, $p < 2 \times 10^{-16}$, $R^2 = 0.5091$). After including Condition (0 = control, 1 = liver fibrosis), EGR1 remained independently associated with FOS (β = 0.9345, SE = 0.1261, $p = 5.21 \times 10^{-12}$), and Condition was also significant (β = −1474.99, SE = 495.95, $p = 0.00335$). The adjusted model showed a significantly improved fit compared with the unadjusted model (ANOVA $p = 0.003353$).

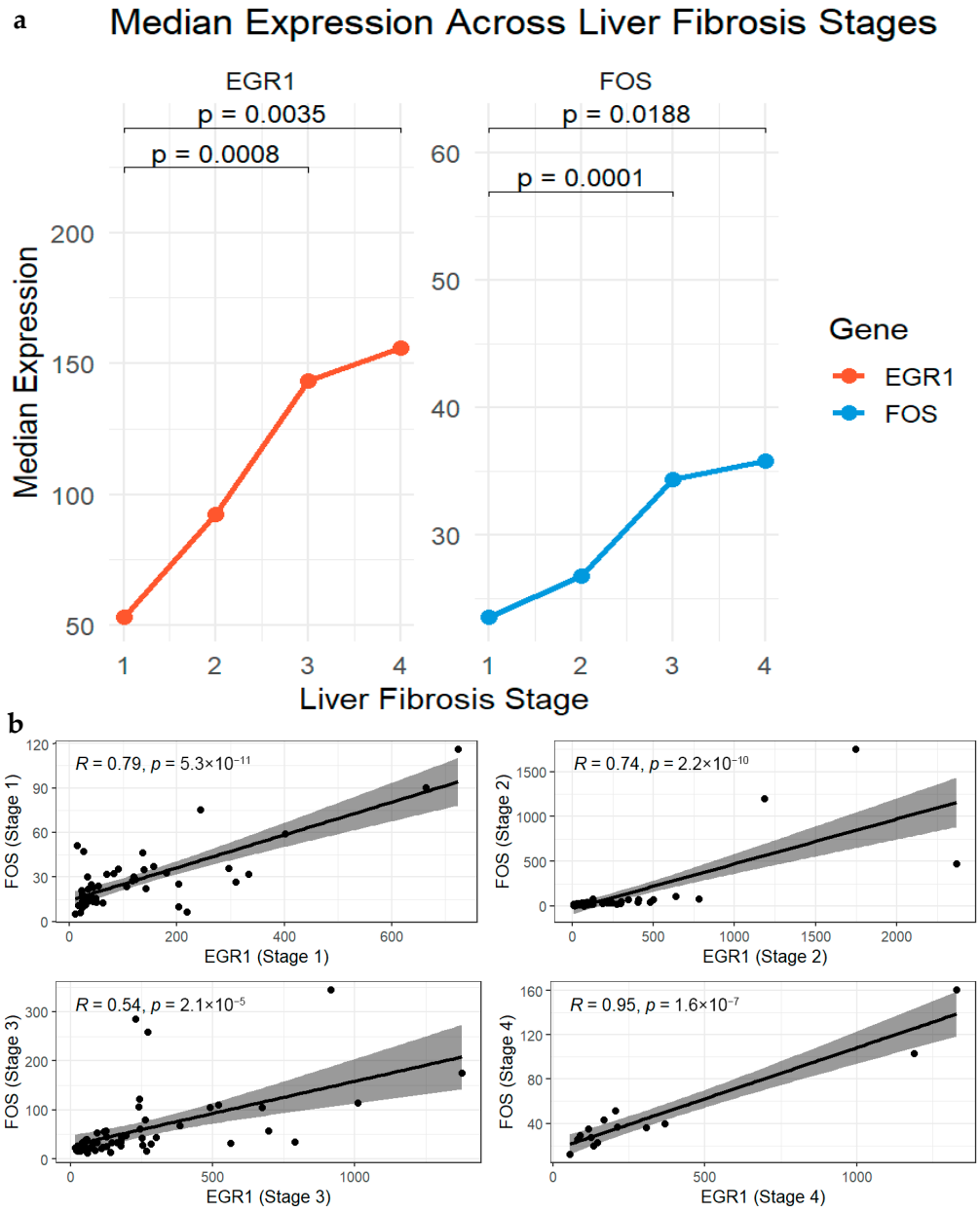


Figure 14. Stage-dependent expression and correlation of EGR1 and FOS in liver fibrosis (GSE135251). (**a**) Median expression of EGR1 and FOS increased progressively across fibrosis stages, with significant differences detected by the Mann–Whitney U test; *p* represents the *p*-value. (**b**) Pearson correlation analysis showed a strong positive association between EGR1 and FOS at all stages; R represents the correlation coefficient, and *p* represents the *p*-value.

Table 5. Stage-wise variation in EGR1 and FOS expression across liver fibrosis progression assessed by the Mann–Whitney U test.

Gene	Comparison	Gene-LF Stage	Median	95% CI for the Median	*p*-Value
EGR1	LF-stage: 1 vs. stage: 2	EGR1-Stage1	53.2538	37.1936 to 118.4480	0.1194
		EGR1-Stage2	92.2395	72.7544 to 133.6347	
EGR1	LF-stage: 1 vs. stage: 3	EGR1-Stage1	53.2538	37.1936 to 118.4480	0.0008
		EGR1-Stage3	143.5478	99.7492 to 237.2930	
EGR1	LF-stage: 1 vs. stage: 4	EGR1-Stage1	53.2538	37.1936 to 118.4480	0.0035
		EGR1-Stage4	155.8706	113.1949 to 312.1864	
FOS	LF-stage: 1 vs. stage: 2	FOS-Stage1	23.5742	16.2270 to 29.6365	0.0667
		FOS-Stage2	26.8092	23.6846 to 33.0759	
FOS	LF-stage: 1 vs. stage: 3	FOS-Stage1	23.5742	16.2270 to 29.6365	0.0001
		FOS-Stage3	34.3894	29.6317 to 43.4834	
FOS	LF-stage: 1 vs. stage: 4	FOS-Stage1	23.5742	16.2270 to 29.6365	0.0188
		FOS-Stage4	35.8047	25.1439 to 44.1809	

4. Discussion

LF represents a pathological reaction to persistent hepatic injury arising from diverse origins, including viral or alcohol-related liver damage, which is marked by activated HSCs and their differentiation into myofibroblast-like cells, causing the hyperdeposition of ECM in the liver [19,20]. Hepatic fibrosis may advance to irreversible stages, including LC and HCC, highlighting the necessity to identify biomarkers in addition to effective therapeutic approaches [21]. The prevention of HSC activation alleviates the fibrotic process, which makes fibrogenic pathways a target for researchers to develop antifibrotic therapies [22].

In our bioinformatic analysis, a hub gene showed an interesting fluctuation in its expression across the different analyzed datasets. This gene is EGR1, a transcription factor that plays a regulatory role in HSC activity. Its expression is influenced by transforming growth factor beta 1 via Smad3 signaling, leading to the expression of bromodomain-containing protein 4, and as a result, activated HSCs, thus enhancing hepatic fibrosis [23]. Conversely, EGR1 serves a protective function in the liver by controlling profibrotic cytokine production during injury; its downregulation can lead to the disruption of PDGF-BB production, thereby reducing the activation of HSCs, an essential event in fibrogenesis [24]. Using an animal model without EGR1 (Egr1 −/−) demonstrated the protective ability of this transcription factor when researchers found that its absence worsened LF. Its downregulation led to higher high-mobility group box 1 concentrations, which stimulated the transition of liver endothelial cells to mesenchymal cells, causing higher collagen deposition and ECM synthesis [25]. This downregulation of EGR1 is not only linked to efficient inflammatory signaling during liver injury but also to the repair process, and it has been found that

its low expression leads to impaired liver repair and regeneration via the reduction in inflammatory signaling, which influences the role of macrophages, the hyperactivation of HSCs, the lack of collagen production regulation, and the intervention of oval cells as an alternative way to resolve the failure of repair during LF [26].

The second downregulated gene identified in our analysis is FOS, which plays a crucial role in hepatic fibrosis and highlights its involvement in liver dysfunction. The c-Fos proto-oncoprotein, a key element of the AP-1 transcriptional complex, has various functions on the cellular level, including proliferation, apoptosis, differentiation and inflammatory processes [27,28]. Chronic liver damage and inflammation lead to hepatic fibrosis, promoting the activation of HSCs and their differentiation into myofibroblast-like cells [29,30]. HSC activation drives excessive deposition of ECM, notably collagen, leading to structural and functional hepatic impairment [31]. Regulation of the ECM interaction with cellular elements is driven by the transcription factor AP-1, highlighting the functional connection with the role of FOS in hepatic fibrosis [31,32]. Previous bioinformatics analyses highlight the essential role of molecular pathways involvement in the pathophysiology of LF, such as PI3K-Akt signaling, ECM-receptor cross-talk, and focal adhesion [33].

AP-1, a transcription factor complex containing FOS and c-FOS, participates in regulating downstream gene transcription triggered by inflammatory stimuli, such as cytokines or growth factors. TGF-β is responsible for the activation of AP-1 during the fibrotic process, which leads to the overexpression of fibrogenic genes. Our findings on the downregulation of FOS may highlight its capacity to impair this process and alleviate LF [34]. The AP-1 transcription factor complex is a key factor in the fibrogenic process, and its activation is mediated by two signaling pathways, mitogen-activated protein kinase (MAPK) and c-Jun N-terminal kinase (JNK). Preventing the activation of AP-1 by downregulating these two pathways can exert an antifibrotic effect [35]. Both FOS and c-Fos, via AP-1, can regulate proinflammatory cytokine expression, and FOS can contribute to this regulation via the NF-κB pathway, which can upregulate its transcription and consequently enhance liver fibrosis by the activation of HSCs [36].

Our findings on FOS downregulation in liver fibrosis are in line with the results conducted on liver sinusoidal endothelial cells, where researchers found that the suppression of the AP-1 transcriptional complex, including FOS, was reported to impair nitric oxide synthesis and vascular homeostasis in hepatic tissue, contributing to an elevation of vascular resistance and diminished blood circulation, and as a result, enhancing the hepatic fibrogenic process, which makes FOS a potential biomarker and therapeutic target in LF [37]. In addition, another study highlighted that suppressing the proliferation of HSCs coincides with decreased FOS expression as an element of AP-1, indicating its participation in the modulation of the fibrogenic signaling via the Ras/ERK pathway [38]. Another study supported our finding in LF, where researchers found that FOS expression is modulated by miR-16; this regulation led to low HSC activation and profibrogenic genes via reducing the role of MAPK/ERK and TGFß/Smad pathways, thus highlighting the protective role of the downregulation of FOS [39]. FOS appears to facilitate tumor progression in HCC via the overexpression of the BORIS gene, which drives tumor cell invasion and migration, in addition to the implication of the Hippo pathway, which governs the proliferation process of cancer cells, clarifying the protective downregulation of FOS not only against LF but also against HCC [40]. FOS has a dual role in liver disease, and bioinformatic analyses have elucidated the oncogenic pathways influenced by FOS in HCC, including the MAPK and G-protein coupled receptor; these pathways are known to be linked to poor prognosis because of recurrence and low survival times, which makes it essential to target the modulation of FOS in liver disease as a therapeutic strategy [41]. Furthermore, FOS is a key regulator of the immune activity, responding to inflammatory signals, which promotes the

tumorigenic process, and participates in oxidative stress caused by metabolic dysfunction of cholesterol through downregulating the nuclear receptor LXRα [42].

To explore in greater detail the immune relevance of EGR1 and FOS in HCC, the TIMER analysis showed that these two genes were positively correlated with multiple immune cell infiltrates, including macrophages, dendritic cells, and T cells, confirming their involvement in immune regulation within the hepatic tumor microenvironment. Similarly, single-cell transcriptomic data confirmed that EGR1 expression was mainly localized in macrophages and dendritic cells, while FOS expression was more widespread, covering macrophages and proliferating T-cell clusters. These observations, which are consistent with the findings of Bai et al., highlight the immune functions of EGR1 and FOS in HCC. However, given the lack of association with overall survival, their role may reflect the dynamics of the immune microenvironment rather than direct oncogenic activity [43].

EGR1 exhibits context-dependent regulation across LF etiologies. In our analysis, EGR1 increased with NAFLD-associated fibrosis yet was markedly reduced in HBV-related fibrosis and in HCC, with stagewise validation in GSE135251 and a strong co-fluctuation with FOS. Mechanistically, EGR1 behaves as an immediate-early, stress-responsive transcription factor that supports adaptive hepatocellular protection during acute injury [44], while functionally coupling with AP-1/FOS signaling implicated in liver disease progression [45] and MAPK/JNK stress cascades central to fibrogenesis [46]. As fibrosis becomes chronic, HSC activation and microenvironmental remodeling dominate [47,48]. Consistently, a study demonstrated that enforced GRK2 expression suppresses EGR1 via inhibition of the IGF1R-ERK/AKT pathway in HCC cells, leading to reduced proliferative and migratory capacity, thereby providing mechanistic support for the progressive decline of EGR1 under chronic or oncogenic signaling [49]. In HBV-associated disease and HCC, persistent viral/oncogenic pressure further suppresses EGR1, consistent with broader tumor-suppressive roles reported for EGR1 [50]. Our findings suggest that metabolic stress can trigger an early rise in EGR1 expression during liver injury, as seen in our first NAFLD dataset [44]. In contrast, prolonged viral infection or oncogenic stress appears to suppress EGR1 activity in HBV-related fibrosis and HCC. This dual behavior highlights the flexible nature of the EGR1-FOS axis, which may adjust its activity according to the underlying etiology and disease stage, linking metabolic adaptation with the fibrogenic and malignant transformation of the liver.

A consistent feature of our analyses is the strong positive correlation between EGR1 and FOS across discovery and validation steps and in HCC, indicating that these transcription factors do not vary independently but instead track a shared program of transcriptional control (Figure 9). This pattern is biologically plausible: in liver injury and regeneration, immediate-early transcription factors are co-induced within hours, and EGR1 rises alongside the AP-1 components JUN/FOS, consistent with a synchronized early response to mitogenic/stress signals [51]. At the level of transcriptional machinery, ERK-dependent immediate-early gene activation jointly engages EGR1 and FOS, providing a mechanistic basis for their coupled induction [52]. In fibrogenic settings, AP-1 activity within HSCs primes chromatin and promotes profibrotic gene expression, supporting a route by which an EGR1-FOS/AP-1 module can sustain fibrogenic transcription over time [53]. Multiomic profiling of human HSCs revealed AP-1 motif enrichment within open chromatin regions near key fibrosis-associated genes, reinforcing the concept of an AP-1-centered regulatory network driving stellate-cell activation [54]. The persistence of the EGR1-FOS correlation across NAFLD stages 1–4 in our external validation aligns with single-cell atlases documenting a conserved HSC activation trajectory across diverse liver injuries [55]. Our enrichment and network analyses suggest that the coordinated EGR1-FOS signal is most likely embedded in an AP-1-centered immediate-early transcriptional program linked

to MAPK/JNK, TGF-β, TNF/NF-κB, growth-factor receptor signaling, and downstream chemokine/cytokine-ECM remodeling pathways. However, this mechanistic interpretation remains inferential and requires experimental confirmation. Potential in vivo strategies to modulate the EGR1-FOS axis include hepatic stellate cell-targeted siRNA/antisense approaches [56] and pharmacologic inhibition of upstream MAPK/JNK/AP-1 signaling [57]. However, because EGR1 appears to have context-dependent functions in experimental liver injury, any therapeutic intervention would likely require cell-type-specific and disease-stage-specific modulation rather than systemic inhibition. Finally, disease-context data are consistent with our findings: EGR1 is frequently suppressed in HCC (tumor-suppressive behavior) [58], while FOS/AP-1 influences hepatic metabolic programs relevant to MASLD, implying that metabolic and inflammatory inputs can together shape the tight coupling of this axis [59]. Taken together, these findings suggest that EGR1 and FOS operate as a flexible regulatory pair that adapts to disease context: showing tight co-activation during early liver injury and regeneration, remaining epigenetically engaged during fibrogenic remodeling, and becoming progressively altered as LF evolves into HCC.

In our study, SOX9 was identified as a shared molecular gene between LF and LC, aligning with previous research that recognized SOX9 as a key factor linking hepatocyte injury to fibrotic remodeling. Experimental evidence demonstrated that the SOX9/lncRNA H19 axis promotes hepatocyte death and fibrosis [60], emphasizing its role at the interface between cellular stress and ECM deposition. A comparative bioinformatics study positioned SOX9 among core genes common to LF and HCC, with increased expression also reported in the CCl_4-induced cirrhosis model [61]. These findings suggest that sustained SOX9 activity may contribute to the progression from chronic fibrogenesis to advanced pathological stages, potentially predisposing to malignant transformation. In addition, the modulation of TGF-β and IL-6 pathways, shown to attenuate fibrotic development [62], supports the notion that SOX9 functions downstream of cytokine-driven signaling cascades. Collectively, these observations highlight SOX9 as a central regulator in hepatic fibrogenesis, integrating inflammatory, regenerative, and stress-responsive pathways.

In our integrative analysis, CD24 emerged as a common molecular signature linking hepatic fibrosis and cirrhosis, consistent with its identification as a marker of activated hepatic progenitor cells during ductular reaction and fibrotic remodeling [63]. Bioinformatic profiling of cirrhotic livers also highlighted the CD24 gene among the key genes co-expressed with immune and extracellular pathways, reinforcing its role at the intersection between inflammation and tissue repair [64]. Functional enrichment studies suggest that CD24-positive progenitor populations contribute to chronic hepatocyte loss and fibrogenic progression, consistent with our finding of their persistence at all advanced stages of the disease. CXCR4 was also identified as a central shared gene, a finding strongly supported by recent mechanistic studies. The first one provided direct human evidence, demonstrating that hypomethylation of the CXCR4 promoter in peripheral blood mononuclear cells serves as a superior diagnostic biomarker for HBV-related hepatic fibrosis/cirrhosis compared to standard clinical scores such as the aspartate aminotransferase-to-platelet ratio index and fibrosis-4 score, underscoring its clinical relevance [65]. Another study reported that the probiotic *Phocaeicola plebeius* ameliorates fibrosis by directly downregulating the expression of profibrotic genes, including CXCR4 [66]. This is further supported by scientists who showed that the antifibrotic compound Senkyunolide I exerts its effect by directly binding to and suppressing CXCR4, thereby inactivating the downstream NLRP3/GSDMD pathway [67]. The translational potential of targeting this receptor is highlighted by researchers who developed a CXCR4-targeted nanomedicine for the precise diagnosis and treatment of LF by delivering drugs to activated hepatic stellate cells [68]. These studies validate CXCR4 as a critical and therapeutically actionable gene in the progression from LF to LC. We

further identified CYP2C19 as a shared gene significantly altered in advanced liver disease, a finding strongly supported by clinical pharmacogenomic studies. Powell et al. provided a molecular validation, demonstrating through RNA-seq that CYP2C19 is significantly downregulated in human NAFLD livers, with expression reduced to 43% in severe fibrosis [69]. This transcriptional suppression translates directly to impaired enzyme function, as evidenced by clinical studies measuring metabolic activity. Researchers confirmed that the enzymatic activity of CYP2C19 is significantly decreased in patients with HCC and LC compared to control patients [70]. This functional decline was observed in another study, which also reported decreased CYP2C19 activity in HCC patients, particularly those with accompanying fibrosis or cirrhosis [71]. Therefore, these shared genes should currently be regarded as candidate biomarkers with varying levels of clinical support depending on the liver disease context. Among them, SOX9 has the strongest direct support in liver fibrosis, as it has been reported to predict progression toward cirrhosis and to correlate with fibrosis severity, supporting its value for fibrosis-stage stratification [72]. CYP2C19 also shows fibrosis-relevant clinical value, since its reduced hepatic expression has been associated with histologically severe NAFLD and may help stratify fibrosis severity [69]. By contrast, CXCR4 is supported mainly as a broader mediator of liver disease progression, including fibrosis, cirrhosis, and HCC, rather than as a directly validated fibrosis-specific diagnostic biomarker [73]. Similarly, the literature on CD24 primarily supports its diagnostic and prognostic relevance in HCC, including poor prognosis, invasiveness, and early diagnostic potential, rather than in liver fibrosis or cirrhosis specifically [74–76].

To our knowledge, this is the first study to focus on the EGR1-FOS axis in LF and its progression to LC and HCC. Our results demonstrate a strong correlation between these transcription factors ($r = 0.77$) and characterize their dynamic expression in different etiologies of LF, showing a significant increase compared to controls despite their overall negative regulation. We also describe fluctuations in their expression during the four stages of LF, confirming that their correlation remains strong throughout the progression of the disease. Furthermore, we show that this pattern of downregulation persists in HCC, highlighting the involvement of this dynamic axis in immune-related functions and elucidating the stability of their correlation and cellular expression, even in cases of advanced HCC. Finally, we identified four genes common to hepatic fibrosis and cirrhosis that could serve as potential biomarkers and therapeutic targets alongside EGR1 and FOS.

Although the datasets were analyzed independently and integrated at the result level, residual inter-dataset heterogeneity related to platform, cohort composition, and sample source may still influence the identified signatures. Therefore, the present findings should be considered exploratory and warrant further validation through independent experimental and clinical studies. Although an adjusted regression analysis was performed using disease status as the available harmonized covariate, broader multivariable adjustment for clinical confounders was not possible due to limited patient-level metadata in the public dataset. Since the present work was designed as a computational transcriptomic study, no functional experiments, such as EGR1/FOS knockdown or overexpression, were performed. Therefore, the mechanistic roles of these genes in liver fibrosis need to be confirmed through future in vitro and in vivo studies.

5. Conclusions

Our study allowed us to identify a novel dynamic EGR1-FOS axis involved in LF and its progression to LC and HCC, using multiple datasets across these disease stages. The expression pattern of EGR1 showed dependence on both the underlying etiology of LF and the degree of disease advancement, and it appeared to be coregulated with FOS throughout fibrosis progression and into HCC. These findings provide a useful basis for developing

precision-medicine approaches for diagnosis and potential therapeutic targeting of the EGR1-FOS axis, along with the four shared genes identified in this work. Given the importance of these results, further in vitro and in vivo studies are needed to validate our observations. A deeper understanding of the mechanisms driving the fluctuations in EGR1 expression will be essential to harness the therapeutic potential of this axis in LF and its progression.

Supplementary Materials: The following supporting information can be downloaded at: https://www.mdpi.com/article/10.3390/biomedinformatics6030023/s1, Figure S1: Normalization of liver fibrosis and cirrhosis transcriptomic datasets.

Author Contributions: Conceptualization, Y.N., H.E., A.O., H.N., M.N. and M.M.; Data curation, Y.N., H.E., A.O., H.N., R.E., M.A.L., I.F., M.N. and M.M.; Formal analysis, Y.N., H.E., A.O., H.N., R.E., M.A.L., I.F., M.N. and M.M.; Writing—review and editing, Y.N., H.E., A.O., H.N., R.E., M.A.L., I.F., M.N. and M.M.; Writing—original draft, Y.N.; Methodology, Y.N., H.N., M.N. and M.M.; Investigation, Y.N., M.N. and M.M.; Software, Y.N., A.O., M.N. and M.M.; Supervision, M.N. and M.M.; Validation, M.N. and M.M. All authors have read and agreed to the published version of the manuscript.

Funding: This research received no external funding.

Institutional Review Board Statement: Not applicable.

Informed Consent Statement: Not applicable.

Data Availability Statement: All data generated or analyzed during this study are included in this published article and its Supplementary Materials.

Acknowledgments: We gratefully acknowledge the researchers who made their transcriptomic datasets publicly available through repositories such as GEO. Their commitment to open data and collaborative science made this integrative analysis possible and greatly contributed to the insights achieved in our study.

Conflicts of Interest: The authors declare no conflicts of interest.

Abbreviations

The following abbreviations are used in this manuscript:

LF	Liver Fibrosis
LC	Liver Cirrhosis
HCC	Hepatocellular Carcinoma
LIHC	Liver Hepatocellular Carcinoma
ECM	Extracellular Matrix
HSCs	Hepatic Stellate Cells
GEO	Gene Expression Omnibus
DEGs	Differentially Expressed Genes
GEPIA	Gene Expression Profiling Interactive Analysis
HBV	Hepatitis B Virus
NAFLD	Non-Alcoholic Fatty Liver Disease
BP	Biological Processes
MF	Molecular Functions
CC	Cellular Components
STRING	Search Tool for the Retrieval of Interacting Genes
MCC	Maximal Clique Centrality
EPC	Edge Percolated Component
TCGA	The Cancer Genome Atlas
GTEx	GenotypeTissue Expression
UMAP	Uniform Manifold Approximation and Projection

TIMER	Tumor IMmune Estimation Resource
SCNA	Somatic Copy Number Alteration
GO	Gene Ontology
KEGG	Kyoto Encyclopedia of Genes and Genomes
MAPK	Mitogen-Activated Protein Kinase
JNK	C-Jun N-Terminal Kinase
TISCH2	Tumor Immune Single-cell Hub 2
HR	Hazard Ratio
PPI	Protein–Protein Interaction

References

1. Yu, L.; Gao, F.; Li, Y.; Su, D.; Han, L.; Li, Y.; Zhang, X.; Feng, Z. Role of Pattern Recognition Receptors in the Development of MASLD and Potential Therapeutic Applications. *Biomed. Pharmacother.* **2024**, *175*, 116724. [CrossRef] [PubMed]
2. Taru, V.; Szabo, G.; Mehal, W.; Reiberger, T. Inflammasomes in Chronic Liver Disease: Hepatic Injury, Fibrosis Progression and Systemic Inflammation. *J. Hepatol.* **2024**, *81*, 895–910. [CrossRef] [PubMed]
3. Elpek, G.Ö. Cellular and Molecular Mechanisms in the Pathogenesis of Liver Fibrosis: An Update. *World J. Gastroenterol. WJG* **2014**, *20*, 7260–7276. [CrossRef] [PubMed]
4. Liu, Q.; Li, J.; Li, X.; Zhang, L.; Yao, S.; Wang, Y.; Tuo, B.; Jin, H. Advances in the Understanding of the Role and Mechanism of Action of PFKFB3-Mediated Glycolysis in Liver Fibrosis (Review). *Int. J. Mol. Med.* **2024**, *54*, 105. [CrossRef]
5. Juanola, A.; Pose, E.; Ginès, P. Liver Cirrhosis: Ancient Disease, New Challenge. *Med. Clínica Engl. Ed.* **2025**, *164*, 238–246. [CrossRef]
6. Fadlallah, H.; El Masri, D.; Bahmad, H.F.; Abou-Kheir, W.; El Masri, J. Update on the Complications and Management of Liver Cirrhosis. *Med. Sci.* **2025**, *13*, 13. [CrossRef]
7. Holland, C.H.; Ramirez Flores, R.O.; Myllys, M.; Hassan, R.; Edlund, K.; Hofmann, U.; Marchan, R.; Cadenas, C.; Reinders, J.; Hoehme, S.; et al. Transcriptomic Cross-Species Analysis of Chronic Liver Disease Reveals Consistent Regulation Between Humans and Mice. *Hepatol. Commun.* **2022**, *6*, 161. [CrossRef]
8. Jiang, C.; Li, P.; Ruan, X.; Ma, Y.; Kawai, K.; Suemizu, H.; Cao, H. Comparative Transcriptomics Analyses in Livers of Mice, Humans, and Humanized Mice Define Human-Specific Gene Networks. *Cells* **2020**, *9*, 2566. [CrossRef]
9. Graupera, I.; Isus, L.; Coll, M.; Pose, E.; Díaz, A.; Vallverdú, J.; Rubio-Tomás, T.; Martínez-Sánchez, C.; Huelin, P.; Llopis, M.; et al. Molecular Characterization of Chronic Liver Disease Dynamics: From Liver Fibrosis to Acute-on-Chronic Liver Failure. *JHEP Rep. Innov. Hepatol.* **2022**, *4*, 100482. [CrossRef]
10. Wang, M.; Gong, Q.; Zhang, J.; Chen, L.; Zhang, Z.; Lu, L.; Yu, D.; Han, Y.; Zhang, D.; Chen, P.; et al. Characterization of Gene Expression Profiles in HBV-Related Liver Fibrosis Patients and Identification of ITGBL1 as a Key Regulator of Fibrogenesis. *Sci. Rep.* **2017**, *7*, 43446. [CrossRef]
11. Moylan, C.A.; Pang, H.; Dellinger, A.; Suzuki, A.; Garrett, M.E.; Guy, C.D.; Murphy, S.K.; Ashley-Koch, A.E.; Choi, S.S.; Michelotti, G.A.; et al. Hepatic Gene Expression Profiles Differentiate Presymptomatic Patients with Mild versus Severe Nonalcoholic Fatty Liver Disease. *Hepatology* **2014**, *59*, 471–482. [CrossRef]
12. Mas, V.R.; Maluf, D.G.; Archer, K.J.; Yanek, K.; Kong, X.; Kulik, L.; Freise, C.E.; Olthoff, K.M.; Ghobrial, R.M.; McIver, P.; et al. Genes Involved in Viral Carcinogenesis and Tumor Initiation in Hepatitis C Virus-Induced Hepatocellular Carcinoma. *Mol. Med. Camb. Mass* **2009**, *15*, 85–94. [CrossRef]
13. Shen, Q.; Eun, J.W.; Lee, K.; Kim, H.S.; Yang, H.D.; Kim, S.Y.; Lee, E.K.; Kim, T.; Kang, K.; Kim, S.; et al. Barrier to Autointegration Factor 1, Procollagen-Lysine, 2-Oxoglutarate 5-Dioxygenase 3, and Splicing Factor 3b Subunit 4 as Early-Stage Cancer Decision Markers and Drivers of Hepatocellular Carcinoma. *Hepatology* **2018**, *67*, 1360–1377. [CrossRef]
14. Schulze, K.; Imbeaud, S.; Letouzé, E.; Alexandrov, L.B.; Calderaro, J.; Rebouissou, S.; Couchy, G.; Meiller, C.; Shinde, J.; Soysouvanh, F.; et al. Exome Sequencing of Hepatocellular Carcinomas Identifies New Mutational Signatures and Potential Therapeutic Targets. *Nat. Genet.* **2015**, *47*, 505–511. [CrossRef] [PubMed]
15. Ma, J.; Gui, H.; Tang, Y.; Ding, Y.; Qian, G.; Yang, M.; Wang, M.; Song, X.; Lv, H. In Silico Identification of 10 Hub Genes and an miRNA–mRNA Regulatory Network in Acute Kawasaki Disease. *Front. Genet.* **2021**, *12*, 585058. [CrossRef] [PubMed]
16. Tang, Z.; Li, C.; Kang, B.; Gao, G.; Li, C.; Zhang, Z. GEPIA: A Web Server for Cancer and Normal Gene Expression Profiling and Interactive Analyses. *Nucleic Acids Res.* **2017**, *45*, W98–W102. [CrossRef]
17. Li, T.; Fan, J.; Wang, B.; Traugh, N.; Chen, Q.; Liu, J.S.; Li, B.; Liu, X.S. TIMER: A Web Server for Comprehensive Analysis of Tumor-Infiltrating Immune Cells. *Cancer Res.* **2017**, *77*, e108–e110. [CrossRef]

18. Govaere, O.; Cockell, S.; Tiniakos, D.; Queen, R.; Younes, R.; Vacca, M.; Alexander, L.; Ravaioli, F.; Palmer, J.; Petta, S.; et al. Transcriptomic Profiling across the Nonalcoholic Fatty Liver Disease Spectrum Reveals Gene Signatures for Steatohepatitis and Fibrosis. *Sci. Transl. Med.* **2020**, *12*, eaba4448. [CrossRef] [PubMed]
19. Wang, F.-D.; Zhou, J.; Chen, E.-Q. Molecular Mechanisms and Potential New Therapeutic Drugs for Liver Fibrosis. *Front. Pharmacol.* **2022**, *13*, 787748. [CrossRef]
20. Khomich, O.; Ivanov, A.V.; Bartosch, B. Metabolic Hallmarks of Hepatic Stellate Cells in Liver Fibrosis. *Cells* **2020**, *9*, 24. [CrossRef]
21. Berumen, J.; Baglieri, J.; Kisseleva, T.; Mekeel, K. Liver Fibrosis: Pathophysiology and Clinical Implications. *WIREs Mech. Dis.* **2021**, *13*, e1499. [CrossRef]
22. Tan, Z.; Sun, H.; Xue, T.; Gan, C.; Liu, H.; Xie, Y.; Yao, Y.; Ye, T. Liver Fibrosis: Therapeutic Targets and Advances in Drug Therapy. *Front. Cell Dev. Biol.* **2021**, *9*, 730176. [CrossRef]
23. Tian, H.; Xu, F.; Zhao, F.; Pan, N.; Lu, S.; Jia, X.; Zhou, Y. Early-Immediate Gene Egr1 Is Associated with TGFβ1 Regulation of Epigenetic Reader Bromodomain-Containing Protein 4 via the Canonical Smad3 Signaling in Hepatic Stellate Cells in Vitro and in Vivo. *FASEB J. Off. Publ. Fed. Am. Soc. Exp. Biol.* **2022**, *36*, e22605. [CrossRef] [PubMed]
24. Wang, Y.; Wang, P.; Yu, Y.; Huang, E.; Yao, Y.; Guo, D.; Peng, H.; Tian, B.; Zheng, Q.; Jia, M.; et al. Hepatocyte Ninjurin2 Promotes Hepatic Stellate Cell Activation and Liver Fibrosis through the IGF1R/EGR1/PDGF-BB Signaling Pathway. *Metabolism* **2023**, *140*, 155380. [CrossRef]
25. Wei, M.; Zhang, Y.; Zhang, H.; Huang, Z.; Miao, H.; Zhang, T.; Lu, B.; Ji, L. HMGB1 Induced Endothelial to Mesenchymal Transition in Liver Fibrosis: The Key Regulation of Early Growth Response Factor 1. *Biochim. Biophys. Acta BBA-Gen. Subj.* **2022**, *1866*, 130202. [CrossRef]
26. Pritchard, M.T.; Nagy, L.E. Hepatic Fibrosis Is Enhanced and Accompanied by Robust Oval Cell Activation after Chronic Carbon Tetrachloride Administration to Egr-1-Deficient Mice. *Am. J. Pathol.* **2010**, *176*, 2743–2752. [CrossRef] [PubMed]
27. Güller, M.C.; André, J.; Legrand, A.; Setterblad, N.; Mauviel, A.; Verrecchia, F.; Daniel, F.; Bernuau, D. c-Fos Accelerates Hepatocyte Conversion to a Fibroblastoid Phenotype through ERK-mediated Upregulation of paxillin-Serine178 Phosphorylation. *Mol. Carcinog.* **2009**, *48*, 532–544. [CrossRef] [PubMed]
28. Mikula, M.; Gotzmann, J.; Fischer, A.N.M.; Wolschek, M.F.; Thallinger, C.; Schulte-Hermann, R.; Beug, H.; Mikulits, W. The Proto-Oncoprotein c-Fos Negatively Regulates Hepatocellular Tumorigenesis. *Oncogene* **2003**, *22*, 6725–6738. [CrossRef]
29. Akkız, H.; Gieseler, R.K.; Canbay, A. Liver Fibrosis: From Basic Science towards Clinical Progress, Focusing on the Central Role of Hepatic Stellate Cells. *Int. J. Mol. Sci.* **2024**, *25*, 7873. [CrossRef]
30. Zhang, D.; Zhang, Y.; Sun, B. The Molecular Mechanisms of Liver Fibrosis and Its Potential Therapy in Application. *Int. J. Mol. Sci.* **2022**, *23*, 12572. [CrossRef]
31. Ortiz, C.; Schierwagen, R.; Schaefer, L.; Klein, S.; Trepat, X.; Trebicka, J. Extracellular Matrix Remodeling in Chronic Liver Disease. *Curr. Tissue Microenviron. Rep.* **2021**, *2*, 41–52. [CrossRef]
32. Yan, Y.; Zeng, J.; Xing, L.; Li, C. Extra- and Intra-Cellular Mechanisms of Hepatic Stellate Cell Activation. *Biomedicines* **2021**, *9*, 1014. [CrossRef] [PubMed]
33. Yang, X.; Cheng, Q.-N.; Wu, J.-F.; Ai, W.-B.; Ma, L. Analysis of Key Genes and Related Transcription Factors in Liver Fibrosis Based on Bioinformatic Technology. *Int. J. Clin. Exp. Pathol.* **2021**, *14*, 444–454. [PubMed]
34. Miyahara, T.; Schrum, L.; Rippe, R.; Xiong, S.; Yee, H.F.; Motomura, K.; Anania, F.A.; Willson, T.M.; Tsukamoto, H. Peroxisome Proliferator-Activated Receptors and Hepatic Stellate Cell Activation. *J. Biol. Chem.* **2000**, *275*, 35715–35722. [CrossRef]
35. Bataller, R.; Schwabe, R.F.; Choi, Y.H.; Yang, L.; Paik, Y.H.; Lindquist, J.; Qian, T.; Schoonhoven, R.; Hagedorn, C.H.; Lemasters, J.J.; et al. NADPH Oxidase Signal Transduces Angiotensin II in Hepatic Stellate Cells and Is Critical in Hepatic Fibrosis. *J. Clin. Investig.* **2003**, *112*, 1383–1394. [CrossRef]
36. Zhang, Z.; Gao, Z.; Hu, W.; Yin, S.; Wang, C.; Zang, Y.; Chen, J.; Zhang, J.; Dong, L. 3,3′-Diindolylmethane Ameliorates Experimental Hepatic Fibrosis via Inhibiting miR-21 Expression. *Br. J. Pharmacol.* **2013**, *170*, 649–660. [CrossRef]
37. Su, T.; Yang, Y.; Lai, S.; Jeong, J.; Jung, Y.; McConnell, M.; Utsumi, T.; Iwakiri, Y. Single-Cell Transcriptomics Reveals Zone-Specific Alterations of Liver Sinusoidal Endothelial Cells in Cirrhosis. *Cell. Mol. Gastroenterol. Hepatol.* **2021**, *11*, 1139–1161. [CrossRef]
38. Liu, X.-J. Effects of the Tyrosine Protein Kinase Inhibitor Genistein on the Proliferation, Activation of Cultured Rat Hepatic Stellate Cells. *World J. Gastroenterol.* **2002**, *8*, 739. [CrossRef]
39. Pan, Q.; Guo, C.; Sun, C.; Fan, J.; Fang, C. Integrative Analysis of the Transcriptome and Targetome Identifies the Regulatory Network of miR-16: An Inhibitory Role against the Activation of Hepatic Stellate Cells. *Biomed. Mater. Eng.* **2014**, *24*, 3863–3871. [CrossRef] [PubMed]
40. Xian, L.; Xiong, Y.; Qin, L.; Wei, L.; Zhou, S.; Wang, Q.; Fu, Q.; Chen, M.; Qin, Y. Jun/Fos Promotes Migration and Invasion of Hepatocellular Carcinoma Cells by Enhancing BORIS Promoter Activity. *Int. J. Biochem. Cell Biol.* **2024**, *169*, 106540. [CrossRef]
41. Hu, J.-W.; Ding, G.-Y.; Fu, P.-Y.; Tang, W.-G.; Sun, Q.-M.; Zhu, X.-D.; Shen, Y.-H.; Zhou, J.; Fan, J.; Sun, H.-C.; et al. Identification of FOS as a Candidate Risk Gene for Liver Cancer by Integrated Bioinformatic Analysis. *BioMed Res. Int.* **2020**, *2020*, 6784138. [CrossRef] [PubMed]

42. Bakiri, L.; Hamacher, R.; Graña, O.; Guío-Carrión, A.; Campos-Olivas, R.; Martinez, L.; Dienes, H.P.; Thomsen, M.K.; Hasenfuss, S.C.; Wagner, E.F. Liver Carcinogenesis by FOS-Dependent Inflammation and Cholesterol Dysregulation. *J. Exp. Med.* **2017**, *214*, 1387–1409. [CrossRef] [PubMed]
43. Bai, Q.; Liu, H.; Guo, H.; Lin, H.; Song, X.; Jin, Y.; Liu, Y.; Guo, H.; Liang, S.; Song, R.; et al. Identification of Hub Genes Associated with Development and Microenvironment of Hepatocellular Carcinoma by Weighted Gene Co-Expression Network Analysis and Differential Gene Expression Analysis. *Front. Genet.* **2020**, *11*, 615308. [CrossRef]
44. Lei, X.; Xu, Q.; Li, C.; Niu, B.; Ming, Y.; Li, J.; Tang, Y.; Li, X.; Tang, J.; Wu, J.; et al. Egr1 Confers Protection against Acetaminophen-induced Hepatotoxicity via Transcriptional Upregulating of Acaa2. *Int. J. Biol. Sci.* **2022**, *18*, 3800–3817. [CrossRef]
45. Villarruel-Melquiades, F.; Aguirre-Maldonado, I.; Herrera-López, E.E.; Mendoza-Garrido, M.E.; Pérez-Carreón, J.I.; Bañuelos, C.; Camacho, J. Activator Protein-1 in Liver Pathology: From Precancerous Diseases to Hepatocellular Carcinoma. *Hepatoma Res.* **2024**, *10*, 51. [CrossRef]
46. Hao, M.; Lu, Y.; Yao, Z.; Wang, P.; Chen, Z.; Zhou, L.; Yang, Q.; Sang, X.; Wang, K.; Cao, G. The Role of JNK Signaling Pathway in Organ Fibrosis. *J. Adv. Res.* **2025**, *74*, 207–223. [CrossRef] [PubMed]
47. Nevzorova, Y.A.; Weiskirchen, R.; Liedtke, C. Mouse Models for Hepatic Stellate Cell Activation and Liver Fibrosis Initiation. In *Hepatic Stellate Cells*; Methods in Molecular Biology; Humana: New York, NY, USA, 2023; Volume 2669, pp. 177–191. [CrossRef]
48. Wang, L.; Huang, Y.; Chen, J.; Gao, J.; Chen, S.; Zhao, M.; Lin, J.; Zhou, S.; Shen, Y.; Cheng, Y. Dynamic Crosstalk between HSCs and Liver Microenvironment: Multicellular Interactions in the Regulation of Liver Fibrosis. *Front. Cell Dev. Biol.* **2025**, *13*, 1635763. [CrossRef]
49. Ma, Y.; Han, C.-C.; Huang, Q.; Sun, W.-Y.; Wei, W. GRK2 Overexpression Inhibits IGF1-Induced Proliferation and Migration of Human Hepatocellular Carcinoma Cells by Downregulating EGR1. *Oncol. Rep.* **2016**, *35*, 3068–3074. [CrossRef]
50. Shimojukkoku, Y.; Nguyen, P.T.; Ishihata, K.; Ishida, T.; Kajiya, Y.; Oku, Y.; Kawaguchi, K.; Tsuchiyama, T.; Saijo, H.; Shima, K.; et al. Role of Early Growth Response-1 as a Tumor Suppressor in Oral Squamous Cell Carcinoma. *Discov. Oncol.* **2024**, *15*, 714. [CrossRef]
51. Llorens-Giralt, P.; Ruiz-Romero, M.; Nurtdinov, R.; Herranz-Itúrbide, M.; Vicent, G.P.; Serras, F.; Fabregat, I.; Corominas, M. Sequential Activation of Transcription Factors Promotes Liver Regeneration through Specific and Developmental Enhancers. *Cell Genom.* **2025**, *5*, 100887. [CrossRef]
52. Liao, Y.; Shikapwashya, O.N.; Shteyer, E.; Dieckgraefe, B.K.; Hruz, P.W.; Rudnick, D.A. Delayed Hepatocellular Mitotic Progression and Impaired Liver Regeneration in Early Growth Response-1-Deficient Mice. *J. Biol. Chem.* **2004**, *279*, 43107–43116. [CrossRef]
53. Zhao, W.; Yuan, W.; Dong, T.; Qi, W.; Feng, Z.; Li, C.; Sun, Y. Increased Matrix Stiffness Promotes Fibrogenesis of Hepatic Stellate Cells through AP-1-Induced Chromatin Priming. *Commun. Biol.* **2025**, *8*, 920. [CrossRef]
54. Kim, H.Y.; Rosenthal, S.B.; Liu, X.; Miciano, C.; Hou, X.; Miller, M.; Buchanan, J.; Poirion, O.B.; Chilin-Fuentes, D.; Han, C.; et al. Multi-Modal Analysis of Human Hepatic Stellate Cells Identifies Novel Therapeutic Targets for Metabolic Dysfunction-Associated Steatotic Liver Disease. *J. Hepatol.* **2025**, *82*, 882–897. [CrossRef]
55. Merens, V.; Knetemann, E.; Gürbüz, E.; De Smet, V.; Messaoudi, N.; Reynaert, H.; Verhulst, S.; van Grunsven, L.A. Hepatic Stellate Cell Single Cell Atlas Reveals a Highly Similar Activation Process across Liver Disease Aetiologies. *JHEP Rep.* **2025**, *7*, 101223. [CrossRef]
56. Lawitz, E.J.; Shevell, D.E.; Tirucherai, G.S.; Du, S.; Chen, W.; Kavita, U.; Coste, A.; Poordad, F.; Karsdal, M.; Nielsen, M.; et al. BMS-986263 in Patients with Advanced Hepatic Fibrosis: 36-Week Results from a Randomized, Placebo-Controlled Phase 2 Trial. *Hepatology* **2022**, *75*, 912–923. [CrossRef]
57. Kluwe, J.; Pradere, J.-P.; Gwak, G.-Y.; Mencin, A.; De Minicis, S.; Osterreicher, C.H.; Colmenero, J.; Bataller, R.; Schwabe, R.F. Modulation of Hepatic Fibrosis by C-Jun-N-Terminal Kinase Inhibition. *Gastroenterology* **2010**, *138*, 347–359. [CrossRef]
58. Pan, M.; Luo, M.; Liu, L.; Chen, Y.; Cheng, Z.; Wang, K.; Huang, L.; Tang, N.; Qiu, J.; Huang, A.; et al. EGR1 Suppresses HCC Growth and Aerobic Glycolysis by Transcriptionally Downregulating PFKL. *J. Exp. Clin. Cancer Res.* **2024**, *43*, 35. [CrossRef]
59. Li, A.; Gilglioni, E.H.; St-Pierre-Wijckmans, W.; Hosseinzadeh, L.; Veyrat-Durebex, C.; Singh, S.P.; Coppari, R.; Bakiri, L.; Gurzov, E.N. Nutritional C-Fos Induction Rewires Hepatic Metabolism and Can Promote Obesity-Associated Hepatocellular Carcinoma. *Adv. Sci.* **2025**, *12*, e09755. [CrossRef] [PubMed]
60. Wang, C.; Deng, J.; Deng, H.; Kang, Z.; Huang, Z.; Ding, Z.; Dong, L.; Chen, J.; Zhang, J.; Zang, Y. A Novel Sox9/lncRNA H19 Axis Contributes to Hepatocyte Death and Liver Fibrosis. *Toxicol. Sci.* **2020**, *177*, 214–225. [CrossRef] [PubMed]
61. Li, Y.; Yuan, S.-L.; Yin, J.-Y.; Yang, K.; Zhou, X.-G.; Xie, W.; Wang, Q. Differences of Core Genes in Liver Fibrosis and Hepatocellular Carcinoma: Evidence from Integrated Bioinformatics and Immunohistochemical Analysis. *World J. Gastrointest. Oncol.* **2022**, *14*, 1265–1280. [CrossRef] [PubMed]
62. Šisl, D.; Flegar, D.; Filipović, M.; Turčić, P.; Planinić, P.; Šućur, A.; Kovačić, N.; Grčević, D.; Kelava, T. Tamoxifen Ameliorates Cholestatic Liver Fibrosis in Mice: Upregulation of TGFβ and IL6 Is a Potential Protective Mechanism. *Biomedicines* **2022**, *10*, 1209. [CrossRef]

63. Huang, W.-J.; Qiu, B.-J.; Qi, X.-S.; Chen, C.-Y.; Liu, W.-M.; Zhou, S.; Ding, M.; Lu, F.-F.; Zhao, J.; Tang, D.; et al. CD24+LCN2+ Liver Progenitor Cells in Ductular Reaction Contributed to Macrophage Inflammatory Responses in Chronic Liver Injury. *Cell Biosci.* **2023**, *13*, 184. [CrossRef]
64. Tai, Y.; Zhao, C.; Gao, J.; Lan, T.; Tong, H. Identification of miRNA-Target Gene Regulatory Networks in Liver Fibrosis Based on Bioinformatics Analysis. *PeerJ* **2021**, *9*, e11910. [CrossRef]
65. Chen, N.; Sun, Y.; Luo, P.; Tang, Y.; Fan, Y.; Han, L.; Wang, K. Association of CXCR4 Gene Expression and Promoter Methylation with Chronic Hepatitis B-Related Fibrosis/Cirrhosis. *Int. Immunopharmacol.* **2024**, *139*, 112686. [CrossRef]
66. Sharma, S.P.; Cha, M.-G.; Kwon, G.-H.; Song, S.H.; Park, J.H.; Kim, M.J.; Eom, J.A.; Lee, K.J.; Yoon, S.J.; Park, H.; et al. *Phocaeicola plebeius* Oral Treatment Improve Fibrosis by Reversing Cirrhosis-Related Hepatic Gene Dysregulation. *Life Sci.* **2025**, *381*, 123979. [CrossRef] [PubMed]
67. Wang, K.; Yang, Y.; Yue, B.; Li, M.; Chen, C.; Du, J.; Long, F. Senkyunolide I Targets CXCR4 to Attenuate Liver Fibrosis via Suppression of the NLRP3/GSDMD Pathway. *Int. Immunopharmacol.* **2025**, *164*, 115348. [CrossRef]
68. Wang, L.; Zhou, J.; Wang, J.; Wang, X.; Dong, H.; Zhao, L.; Wu, J.; Peng, J. Hepatic Stellate Cell-Targeting Micelle Nanomedicine for Early Diagnosis and Treatment of Liver Fibrosis. *Adv. Healthc. Mater.* **2024**, *13*, e2303710. [CrossRef]
69. Powell, N.R.; Liang, T.; Ipe, J.; Cao, S.; Skaar, T.C.; Desta, Z.; Qian, H.-R.; Ebert, P.J.; Chen, Y.; Thomas, M.K.; et al. Clinically Important Alterations in Pharmacogene Expression in Histologically Severe Nonalcoholic Fatty Liver Disease. *Nat. Commun.* **2023**, *14*, 1474. [CrossRef] [PubMed]
70. Zhou, J.; Gao, N.; Tian, X.; Fang, Y.; Gao, J.; Wen, Q.; Cui, M.-Z.; Zhang, Y.-F.; Li, S.-F.; Jia, L.-J.; et al. Liver Microsomal Protein Content and Activity in Patients with Hepatocellular Carcinoma and Cirrhosis: Implications for the in Vivo Prediction of Individual Hepatic Clearance. *J. Gastrointest. Oncol.* **2025**, *16*, 146–158. [CrossRef] [PubMed]
71. Zhou, J.; Wen, Q.; Li, S.-F.; Zhang, Y.-F.; Gao, N.; Tian, X.; Fang, Y.; Gao, J.; Cui, M.-Z.; He, X.-P.; et al. Significant Change of Cytochrome P450s Activities in Patients with Hepatocellular Carcinoma. *Oncotarget* **2016**, *7*, 50612–50623. [CrossRef]
72. Athwal, V.S.; Pritchett, J.; Llewellyn, J.; Martin, K.; Camacho, E.; Raza, S.M.; Phythian-Adams, A.; Birchall, L.J.; Mullan, A.F.; Su, K.; et al. SOX9 Predicts Progression toward Cirrhosis in Patients While Its Loss Protects against Liver Fibrosis. *EMBO Mol. Med.* **2017**, *9*, 1696–1710. [CrossRef]
73. Wang, S.; Gao, S.; Li, Y.; Qian, X.; Luan, J.; Lv, X. Emerging Importance of Chemokine Receptor CXCR4 and Its Ligand in Liver Disease. *Front. Cell Dev. Biol.* **2021**, *9*, 716842. [CrossRef]
74. Yang, X.-R.; Xu, Y.; Yu, B.; Zhou, J.; Li, J.-C.; Qiu, S.-J.; Shi, Y.-H.; Wang, X.-Y.; Dai, Z.; Shi, G.-M.; et al. CD24 Is a Novel Predictor for Poor Prognosis of Hepatocellular Carcinoma after Surgery. *Clin. Cancer Res. Off. J. Am. Assoc. Cancer Res.* **2009**, *15*, 5518–5527. [CrossRef] [PubMed]
75. Maimaitiming, A.; Zhou, X.; Ma, X.; Huang, Y.; Wang, Q.; Deng, R.; Ren, Y.; Chai, X.; Zhang, P. Clinicopathological and Prognostic Value of Plasma CD24 Level in Hepatocellular Carcinoma. *J. Investig. Surg. Off. J. Acad. Surg. Res.* **2020**, *33*, 536–541. [CrossRef] [PubMed]
76. Rasmy, H.S.; Awad, E.A.; Mohamed, E.S.; Boshra, A.S.; Ibrahim, S.A.M.; Isaac, A. Plasma CD24 Level as a Promising Prognostic Biomarker of Hepatocellular Carcinoma. *Egypt. Liver J.* **2024**, *14*, 36. [CrossRef]

Disclaimer/Publisher's Note: The statements, opinions and data contained in all publications are solely those of the individual author(s) and contributor(s) and not of MDPI and/or the editor(s). MDPI and/or the editor(s) disclaim responsibility for any injury to people or property resulting from any ideas, methods, instructions or products referred to in the content.